Some Aspects in the Design of Linear Quadrature Filters for Phase Shifting.

By

Christhian Adonaí González Valdez

A thesis submitted to Centro de Investigaciones en Optica A. C.
for the degree of
Doctor of Philosophy
Department of Optics
April 2012

Typeset in LaTeX 2_ε.

Except where acknowledged in the customary manner, the material presented in this thesis is, to the best of my knowledge, original and has not been submitted in whole or part for a degree in any university.

Christhian Adonaí González Valdez

I dedicate this work to my wife Paty and our baby futurito, who are my inspiration in everything I do and every choice I make.

My Parents Nelsy and Edmundo .∴. , they are the reason why I am here, and made me who I am today.

I also dedicate this to Haret for teaching me that great things in science are born from perseverance and tiny sparks of inspiration.

I would also like to mention Leo and Ariana for their encouragement and support each day in SLP.

Acknowledgments

I would like to thank my supervisors Dr. Manuel Servín Guirado, Dr. Julio Cesar Estrada Rico and Dr. Haret-Codratian Rosu Barbus who introduced me in the science world and their invaluable supervision of this thesis. He encourage me and gave me professional support.

I thank Dr. Luis Adolfo Torres Gonzalez, Martha Gallegos and her family for their helpful, friendship and interest in my professional development.

I acknowledge the support of Centro de Investigaciones en Óptica and Instituto Potosino de Investigación Científica y Tecnológica, and all the attention that I receive from the Academic Department in both CONACYT research center to carry this project to good end.

Last but not least, I want to say thanks to all my friends for their patient and support during the complementation of this thesis.

Christhian Adonaí González Valdez.

Abstract

Phase Shifting Interferometry (PSI) involves a group of experimental methods for retrieving a wave-front phase encoded in the interference fringes. The first step requires the registration of N-frames of fringes ***interferograms***. The frames of fringes are formed by the addition of two wave-fronts, one called the reference, typically a wave-front coming from a flat surface, and a second wave-front reflected by an object under test. The reference wave-front is sequentially shifted in phase from frame to frame taking as reference the first phase distribution of this reference wave-front [1]. ***The phase-shift is based on synchronous detection***, which has been used for a long time in electrical engineering for determining the phase difference between two electrical signals. The synchronous detection uses as reference an incoming sinusoidal signal, the sinusoidal signal is sampled and correlated with a cosinusoidal coming from the object under test [2, 3]. ***The automatic evaluation of interferometric measurements, actually called Phase Shifting Algorithms (PSA) are very popular, because of the rapid evaluation of digital interferometric data by a computer***.

The Phase Shifting Algorithms (PSA), are computer programs created with the objective of obtaining the modulated phase of a signal [4–12]. ***The PSA in fact are based on* complex quadrature filters *in the temporal domain***. The convolution of this filter with the interferometric signal allows the estimation of the modulated phase $\phi(x, y)$. The use of the Fourier Transform applied to the *quadrature filter* function helps to find its spectral response or *frequency transfer function*. The information of the spectral response it is the most valuable information, this because helps to the interpretation and analysis of all of its properties. ***The frequency transfer function of any quadrature filter it is invariant to rotations and reference time shift***[13].

A PSA is designed for phase estimation, the input arguments for its construction differ in the phase-shift values between captured interferograms, in the number of phase steps, and in their sensitivity to the noise [6, 14–20]. An accurate phase-shift is very common due to vibrations, miss-calibration in the experimental set-up, noise due to illumination, tall of these point leads to errors in the measured phase, a phenomenon known as detuning.

The significant addition of this thesis to the theory of PSA is summarized in two points:

- **Given an N-step linear PSA, Which value for the phase-step ω_0 (frequency carrier) among interferograms should be used to obtain the**

least noisy demodulated phase?. In this Thesis, we answer this question in a general way, allowing the possibility to use the close interval $(-\pi, \pi)$. A proper use of the procedure presented in this Thesis (necessarily) involves linear tunable N-step PSA [21].

- **How to design linear tunable N-step PSA that can defeat a detuning in the phase-step ω_0?. In this Thesis we give a general building block and by its consecutive collocation, in the frequency domain, any linear tunable N-step PSA is capable of performing any desired Frequency Transfer Function. This gave a complete control over the signal that is accepted and what signals are filtered out by the linear tunable N-step PSA. This analysis is extended to the harmonics rejection [22].**

Contents

List of Figures

List of Tables

1 Introduction

Linear temporal phase-shifting algorithms (PSA) are widely used to estimate the modulating phase of interferograms [4, 9, 17, 23, 24]. Linear PSA incorporate a constant phase-step ω_0 (in radians/interferogram) to obtain a set of interferometric data [4, 9, 17, 24]. It is well known that the more temporal interferograms we have, the less noisy is the phase that we estimate; for example a *5-step* linear PSA will provide (in general) less noisy phase demodulation than a *3-step* one [11, 13]. However, if we are restricted to take, say 5 temporal interferograms, an interesting piece of information to be aware of is: which value for the phase-step ω_0 should be used in a *5-step* linear PSA to obtain the least noisy demodulated phase ? or which value for the phase-step ω_0 should be used in a *N-step* linear PSA to obtain the least noisy demodulated phase ? Typically $\pi/2$, $2\pi/3$, $\pi/3$ are used and in fact, any phase-step within the open interval $(0, \pi)$ can be employed. In the absence of any measuring noise, all these phase-shifts yield the same estimate for the modulating phase. However, which of these phase-steps ω_0 is the best to obtain the least noisy phase estimation from a temporal set of *3 noisy interferograms* or *N noisy interferograms* ? In this Thesis, working in the frequency space, a general procedure to obtain the optimum phase-step ω_0 of a given linear *N-step* PSA is given. This general procedure is exemplified to some particular linear PSA, notably 3, 5, 7, and *27-step* PSAs. A proper use of the procedure presented in this Thesis (necessarily) involves linear tunable *N-step* PSA.

As it was mentioned before, all PSA takes as input *N phase-shifted* interferometric measures, and give an estimation of their modulating phase. The first and best known PSA designed explicitly to reduce a systematic error source (detuning) was the *5-steps*, Schwider-Hariharan PSA [15]. Since then, dozens of PSAs designed to reduce specific data error sources on the demodulated phase have been published. In Electrical Engineering, the Frequency Transfer Function (FTF) of their linear filters is their standard design tool. Recently the FTF is also being used to design PSAs. In this Thesis, we propose a technique for designing PSA by fine-tuning the few spectral

zeroes of a PSA to approximate a template FTF spectrum. The PSAs spectral zeroes are moved (tuned) while gauging the plot changes on the resulting FTFs magnitude.

Schwider et al. [19] derived the first (and best known) *5-steps* detuning-robust PSI algorithm, and afterwards Hariharan et al. [15] further analysed its properties. In the book of Malacara et al. [9] an encyclopedic number of PSI algorithms are presented, including the motivation behind many of them; their spectral plots are also shown according to Freischlad and Koliopoulos (F&K) [23]. Spectral analysis of PSA was popularized only after the F&K paper [23] was published. Nowadays, spectral analysis is the gold-standard reference to compare among several PSA. Most people uses these spectra to visualize and gauge among several promising PSA, and choose the best one for their needs [7, 20, 23, 25, 26].

More recently Surrel proposed an x-polynomial $P(x)$ associated with a PSA named the Characteristic Polynomial (CP) [11]. The x-polynomial closely follows the Z-transform, or in Surrel's words [11]: "This introduction of a polynomial is similar to what is underlying in the Z-transform theory". That is probably why Surrel preferred the use of x instead of z for his $P(x)$ polynomial. Then, Surrel proposed the CP diagram, to visualize some properties of a PSA based on the (discrete) angular location over the unit circle of these zeroes and their multiplicities [11]. Surrel proposed no continuous spectral plot to gauge his x-polynomials [11], as the F&K spectral plot does provide [23]. He did not follow the standard continuous spectral analysis of Z-transformed digital filters [3].

In 2010, Burke [27] efficiently combined both perspectives: the discrete CP diagram [11], and the continuous F&K spectral analysis [23]. Burke did this to point out the importance of fine-tuning the zeroes of a x-polynomial of *symmetric* PSAs. That is, Burke generated a new visualizing-gauging technique, by combining the discrete CP diagram [11], with the F&K continuous spectrum [23, 27], while finely tuning the PSA' symmetric spectral zeroes.

However, as demonstrated in [4], one drawback of the F&K's spectral analysis [23] is that it changes when the PSI algorithm's reference carrier (the local oscillator) is rotated. Another important drawback of the F&K spectrum is that *only symmetrical PSAs may be F&K spectrally analyzed*. That is because, F&K analysis needs to: "*analyze the spectrum without constant or common phase factors* [19]", and in this way obtain two real functions to plot. We repeat, the F&K spectral analysis can only be made if the PSA is symmetric, such as the ones analyzed by Burke [27], and Larkin *et al* [7], and others [9]. As a consequence, general (non-symmetric) PSAs simply cannot be spectrally analysed using F&K. Briefly, the F&K spectral plot limitations are: a) The spectral plot changes when the local oscillator is phase shifted [4], and b) F&K cannot plot the PSA's spectra of general *non-symmetric* PSAs. These two drawbacks are serious limitation of the F&K spectral analysis technique.

A different perspective of the PSA's theory just discussed was proposed by our group [4], in which a general theory of PSAs based on the Frequency Transfer Function (FTF) $H(\omega)$ is given. The FTF is just the Fourier transform of the impulse response of a digital filter $h(t)$), that is $H(\omega) = F[h(t)]$ [3]; where $F[\cdot]$ is the Fourier Transform. The use of the FTF although new in PSI, has been the standard way of spectral analysis in signal processing engineering for decades [3]. The spectral analysis of PSAs based

on the FTF does not have the limitations of the F&K spectral analysis.

The CP and the FTF perspectives are mathematically equivalent. The x-polynomial follows closely the Z-transform of $h(t)$, while the FTF is the Fourier transform of $h(t)$; both perspectives are related by $\exp(\jmath\omega)$ [3]. The discrete CP diagram associated with the x-polynomial only shows the CP's zeroes and their multiplicities. In other words, the CP diagram shows the behaviour of $H(\omega)$ only at the neighbourhood of the level set $H(\omega) = 0$. Whereas the plot of $|H(\omega)|$ give the continuous, full visualization of the spectral shape including the zeroes shown in a CP diagram. In short, the CP diagram is a visual subset of $H(\omega)$, representing only its behaviour near $H(\omega) = 0$. Note that Surrel [11] could have used the continuous FTF spectral plot $|P\exp(\jmath\omega)|$ for gauging his x-polynomials, but for some reason he did not do that. Therefore, a CP diagram does not provide the full visualizing information provided by $|H(\omega)|$. As a consequence, it is difficult to use the CP diagram for fine-tuning the few zeroes in a PSA. The detailed (continuous) spectral plot provided by $|H(\omega)|$, is paramount to fine-tuning the spectral shape. We need to visualize and gauge the subtle changes in the shape of $|H(\omega)|$ (magnitude of the FTF), to finely tune the PSA spectral zeroes to approximate a target spectrum. Finally note that the target spectrum may be estimated by spectral estimation of experimentally obtained fringe patterns. This real data spectral estimation, and the desired phase noise rejection are the key to know the size N of the PSA.

In this Thesis, just to build a conceptual bridge, we have adopted a combined CP-FTF visualization. But given that the CP diagram is a visual subset of our $|H(\omega)|$ plot, we would not need the CP diagram since the PSA information is within our $|H(\omega)|$ continuous plot.

2 Discrete Time Signals

This Chapter summarizes the linear system theory required for understanding this work. The following chapters make use of the theory presented here.

2.1 Periodic functions and the Spectrum of the signal

A periodic function is one that repeats endlessly with time. Sine waves, triangular waves and square waves are examples of periodic functions. Each periodic function has a period or interval of repetition, related to the frequency as the inverse of it [28]:

$$T = \frac{1}{F}\,. \tag{2.1}$$

These examples of signals represent information. Signals are always assumed to represent useful information. One of the most common signals encountered in nature is that of a sine wave, which is produced by people talking, motion of a pendulum, musical instruments, etc. Signals such as the square wave and triangular wave can be shown to be composed of a combination of sinusoidal waves. The term of*sinusoidal wave* can be applied equally well to sine waves and cosine waves. Thus, sinusoidal waves would be considered to be the building blocks of many other signals [3, 28].

The signals mentioned above are functions of time. The signal amplitude is measured at different time instants, monitoring the *time evolution* (time-domain) of the signal, in others words, how the signal changed with the passage of time. But there are other applications for which another representation is more useful: the *frequency-domain* representation. This representation depicts the amplitudes and frequencies of the constituent sinusoidal waves present in the signal being measured. This representation is also known as the *spectrum of the signal*.

2.2 Analog and Digital Signals

An *analog signal* has an infinity variety of values as time goes. Analog means continuous, so an analog signal is continuous both time and amplitude. During a time interval, an analog signal have any possible value of amplitude between the minimum and maximum limits, for any time inside of the measurement interval. An analog signal measured in a specific instant of time is known as a *discrete time* signal. A discrete time signal has any possible amplitude only at specific points of time, usually equidistant. Thus, just a number of amplitude values are known, at many other moments of time the amplitudes are unknown. Converting an analog signal (continuous-time domain) into a discrete-time signal (discrete time domain) is achieved by a process known as sampling [29].

2.3 Impulse Sampling

A *sampled-data signal* is the result of examining a continuous time signal at periodic T time intervals, Figure 2.1. The sampling rate or sampling frequency is $f_s = 1/T$. Assume that each sample has a width that approaches zero, so the samples will be represented as a sequence of impulse functions [28, 30].

Let $x_s(t)$ represent the sampled data signal and $x(t)$ the original continuous-time signal. The mathematical expression for $x_s(t)$ is:

$$x(t)_s = x(t)p(t)\,, \tag{2.2}$$

where $p(t)$ is the train of impulse functions defined as:

$$p(t) = \sum_{-\infty}^{\infty} \delta(t - nT)\,, \tag{2.3}$$

and $\delta(t)$ is:

$$\delta(t) = \frac{1}{2\pi} \int_{-\infty}^{\infty} \exp(\jmath\omega t) d\omega\,. \tag{2.4}$$

The sampled-data signal $x[t]$ can be expressed as

$$x(t)_s = x(t)p(t) = x(t) \sum_{-\infty}^{\infty} \delta(t - nT)\,, \tag{2.5}$$

the values of $x(t)$ of importance now are those at $t = nT$. Hence, an alternative form for the sampled-data signal is

$$x(t)_s = \sum_{-\infty}^{\infty} x(nT)\delta(t - nT)\,, \tag{2.6}$$

the above equation is composed of a series of equally spaced impulses whose weights represent the values of the original signal at the instants of the sampling points.

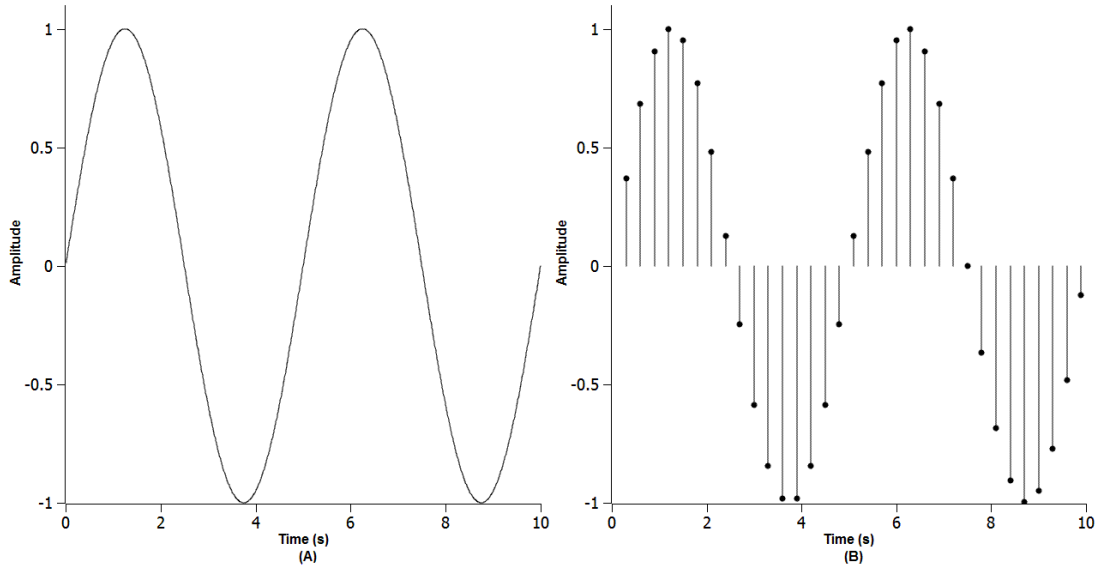

Figure 2.1: (A) Sine continuous time signal with frequency of 2 Hz and unity amplitude. (B) Sine discrete time signal obtained from (A), sampling period of 0.3s

2.4 Digital Signals for What?

The main objective of *Digital Signal Processing* (DSP) essentially deals with signals such as speech, music, video, in other words, any kind of physical quantity that conveys information. These signals take place in analog continuous time form. Given an analog signal, a standard objective is the analysis to obtain useful information. The analog signal is sampled or digitalized and then analysed by using one of the most famous and powerful math tools, *The Fast Fourier Transform (FFT)*. The FFT applied over a signal can reveal several useful parameters about the source of the signal. Evidently the FFT is part of a DSP system that help us to analyse, manipulate and extract information from the input digital signal through the use of a computer.

2.4.1 Discrete Time System

The theory behind DSP is based on a *discrete-time system*. A discrete time system is a transformation that maps a discrete time signal, $x(t)_s$ onto a unique $g(x)$ and it is denoted as: $g(x) = T\{x(t)_s\}$. A very important class of discrete time systems are the *linear time-invariant systems*. A system is said to be linear if obey the following rule [31]:

$$T\{ax_1(t) + bx_2(t)\} = aT\{x_1(t)\} + bT\{x_2(t)\}\,, \tag{2.7}$$

for any constant a and b. A system $T\{\cdot\}$, that maps $x(t)_s$ onto $g(t)$ is said to be *shift* or time-invariant if a shift in the input causes a similar shift at the output:

$$g(t) = T\{x(t)_s\} \Rightarrow g(t - t_0) = T\{x(t - t_0)\}\,. \tag{2.8}$$

From Correlation to Convolution

Correlation algorithms are applied dayly by the brain as tools that allow distinguish among objects. Recognition occurs when the incoming image has a strong match (*correlation*) with an image in memory. The process used in DSP to measure the similarity between two signals is called *Correlation*. When the *correlation* is performed between a signal and itself the process is known as *Autocorrelation*. The *Cross-correlation* is a *correlation* between two different signals. *Correlation* combines three operations [31]:

- Shifting.
- Multiplication.
- Addition.

these three operations are repeated over and over again until the highest accumulative addition is found.

Convolution is very much like *correlation*, but includes the additional operation of flipping. Flipping means the mirror image of a signal about a reference $n = 0$ axis.

- Flipping.
- Shifting.
- Multiplication.
- Addition.

Then repeating these steps over and over again. The main application of *convolution* in DSP is for digital filtering.

In Section 2.3 a discrete time signal was represented as a sequence of numbers. This representation is made in terms of the discrete time unit impulse $\delta(t)$, Equation (2.4). Any discrete time signal can be represented as a sum of scaled and shifted unit impulses:

$$x(t) = \sum_{k=-\infty}^{\infty} x(k)\delta(t-k)\,, \tag{2.9}$$

where $\delta(t-k) = 1$ when $t = k$. If Equation (2.9) is the input of a linear invariant-time system the output $g(t)$ is:

$$g(t) = T\{\sum_{k=-\infty}^{\infty} x(k)\delta(t-k)\}\,, \tag{2.10}$$

by the property of linearity, Equation (2.10) may be rewritten as:

$$g(t) = \sum_{k=-\infty}^{\infty} x(k)T\{\delta(t-k)\}\,, \tag{2.11}$$

by the property of time-invariance, if $h(t)$ is the response to the unit impulse, $\delta(t)$, then the response to $\delta(t-k)$ is simply $h(t-k)$. And now, the above expression can be rewritten as:

$$g(t) = \sum_{k=-\infty}^{\infty} x(k)h(t-k)\,. \tag{2.12}$$

The *unit impulse response*, $h(t) = T\{\delta(t)\}$, of a linear time invariant system fully characterizes that system. More precisely, given the *unit impulse response*, $h(t)$, the output $g(t)$, can be determined for any input, $x(t)$. The sum in Equation (2.12) is commonly called the *convolution sum* and may be expressed more compactly as:

$$g(t) = x(t) * h(t) = \sum_{k=-\infty}^{\infty} x(k)h(t-k)\,. \tag{2.13}$$

2.5 Constructing waves by Sine and Cosine Waves

A periodic signal can be broken down as a combination of sinusoidal signals. This was discovered by Jean Baptiste Joseph Baron de Fourier (1768 - 1830). Sinusoidal waves can be combined together to produce any periodic signal. Figure 2.2 show three sine waves (A), (B) and (C), they all add together to form the fourth sinusoidal wave (D). In this case the fundamental frequency is 3 Hz, the frequency of the second harmonic is 6 Hz, the frequency of the third harmonic is 12 Hz. If the fundamental frequency is denoted by f_1, the equation for the wave in Figure 2.2 (D) results as [31, 32]:

$$s(t) = 6\sin[2\pi(f_1)t] + 4\sin[2\pi(2f_1)t] + 3\sin[2\pi(3f_1)t]\,, \tag{2.14}$$

therefore, $s(t)$ is a combination of a fundamental signal Figure 2.1 (A), second and third harmonics signals, Figures 2.1 (B) and (C). It is important to note that the frequency of the wave in Figure 2.1 (D) is the same as the frequency of the lowest frequency sine wave.

In Figure 2.2 (A-C) all plots started with a zero value at $t = 0$, this leads to the same behaviour in Figure 2.2 (D) i.e., there is no way to create a signal with a non zero value at $t = 0$ by using Equation (2.14). If the *sine* functions is replaced in Equation (2.14) by *cosine* functions, the result will be a signal whose maximum value is localized at $t = 0$. A direct conclusion will be that any periodic signal can be represented by adding *sine* and *cosine* functions of appropriate amplitude and frequency. The periodic signals are combinations of extremely large number of harmonics. Therefore, the general equation can be written as follows:

$$\begin{aligned} s(t) = a_0 + a_1\cos[2\pi(f_1)t] + a_2\cos[2\pi(2f_1)t] + \ldots + a_n\cos[2\pi(nf_1)t] + \\ b_1\sin[2\pi(f_1)t] + b_2\sin[2\pi(2f_1)t] + \ldots + b_n\sin[2\pi(nf_1)t]\,, \end{aligned} \tag{2.15}$$

where a_n represents the amplitudes of *cosine* waves, b_n represents the amplitudes of *sine* waves, nf_1 the fundamental frequency and harmonics and a_0 a shifted upward value to

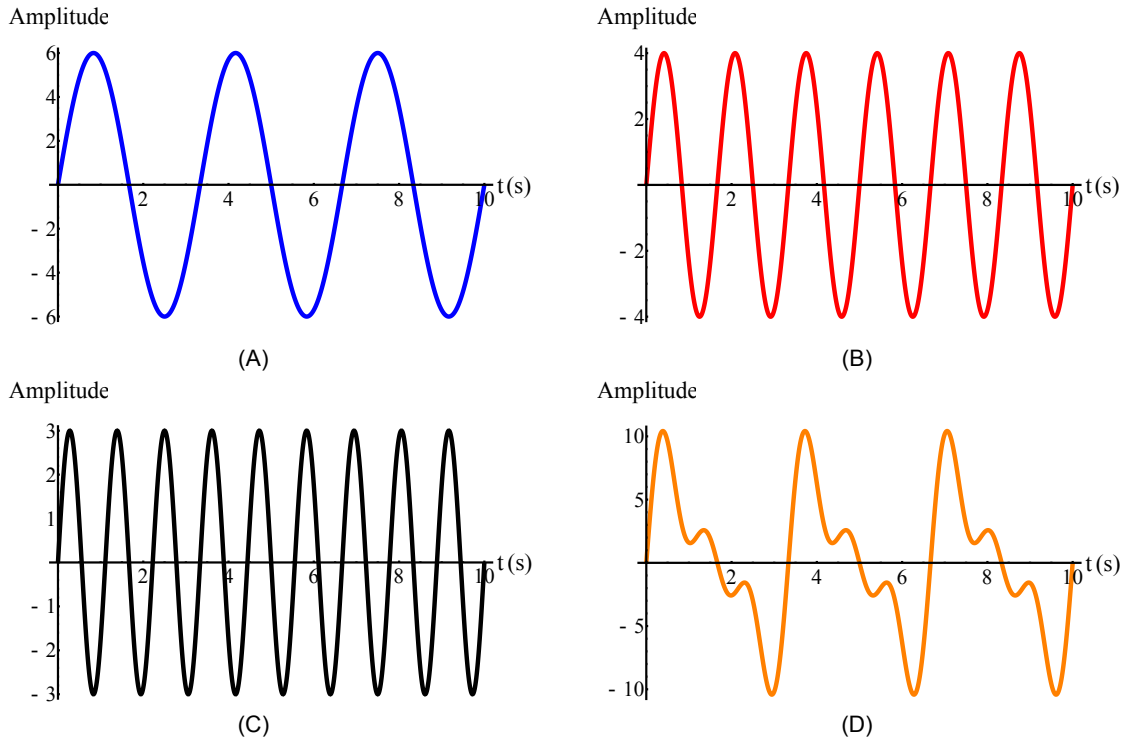

FIGURE 2.2: (A) Sine wave with frequency of 3Hz, amplitude of 6. (B) Sine wave with frequency of 6Hz, amplitude of 4. (C) Sine wave with frequency of 12Hz, amplitude of 3. (D) Adition of sine waves (A), (B), (C). The value at $t = 0$ is 0.

the periodic signal. Equation (2.15) is called a *Fourier Series*. The *sines* and *cosines* with the fundamental frequency and all the corresponding harmonics, are a basis to form all the possible periodic waveforms. In general, the more number of elements in the *Fourier Series* a better construction of the periodic signal results. However, there is an important limitation: if the periodic signal has any discontinuity, e.g. an edge, an infinity number of terms in the *Fourier Series* cannot exactly reconstruct the discontinuity of the signal.

2.6 Fourier Transform

In the previous section, a periodic time signal was derived as a sum of sinusoidal functions, Equation (2.15). The basic signal used as the building block is:

$$A\cos\left(\omega t + \phi\right), \tag{2.16}$$

where A is the amplitude, $\omega = 2\pi f$ is the angular frequency and ϕ is the phase of the sinusoid. When $\phi = \pi/2$, the Equation (2.16) transform into the *sine* function. The exponential function $\exp[\jmath\omega t]$, with ω the angular frequency and $\jmath = \sqrt{-1}$, is simply a

compact notation for describing a vectorial sum of the sine and cosine functions:

$$A\exp(\jmath\omega t) = A\cos(\omega t) + \jmath A\sin(\omega t)\,. \tag{2.17}$$

The *sine* and *cosine* functions can be expressed from Equation (2.17) as:

$$\cos(2\pi nft) = \frac{1}{2}\left(\exp(\jmath 2\pi nft) + \exp(-\jmath 2\pi nft)\right)\,, \tag{2.18}$$

$$\sin(2\pi nft) = \frac{1}{2\jmath}\left(\exp(\jmath 2\pi nft) - \exp(-\jmath 2\pi nft)\right)\,. \tag{2.19}$$

Now, Equation (2.15) can be written as:

$$\begin{aligned} s(t) = \sum_{n=-\infty}^{\infty} a_n \frac{1}{2}\left(\exp(\jmath 2\pi nft) + \exp(-\jmath 2\pi nft)\right) + \\ b_n \frac{1}{2\jmath}\left(\exp(\jmath 2\pi nft) - \exp(-\jmath 2\pi nft)\right)\,, \end{aligned} \tag{2.20}$$

which can be re-written as:

$$s(t) = \sum_{n=-\infty}^{\infty}\left(\frac{1}{2}(a_n - \jmath b_n)\exp(\jmath 2\pi nft) + \frac{1}{2}(b_n + \jmath b_n)\exp(-\jmath 2\pi nft)\right)\,. \tag{2.21}$$

The periodic function just described in Equation (2.15) is represented by a sum of real sinusoidal functions. If the signal to be described is a complex signal, the coefficients a_n and b_n in Equation (2.15) must be complex as represented in Equation (2.21). Using complex exponential functions such as Equation (2.17), the periodic time signal can be written as:

$$s(t) = \sum_{n=-\infty}^{\infty} C_n \exp[\jmath 2\pi nf_1 t]\,, \tag{2.22}$$

with $C_{\pm n} = 1/2(a_n \mp \jmath b_n)$. The coefficients $C_{\pm n}$ can be calculated as:

$$C_{\pm n} = \frac{1}{T}\int_{-\infty}^{\infty} s(t)\exp[\mp\jmath 2\pi nf_1 t]dt\,. \tag{2.23}$$

If the period T of the function $s(t)$ tends to infinity, the separation among the sinusoidal components decrease. This leads to have not just discrete harmonics $\omega = 2\pi nf$, but instead any value for ω is allowed. Now, C_n changes to $C_{2\pi f}$ which leads to the concept of the *Fourier Transform* $\Im[\cdot]$. Let $g(t)$ be a continuous function, the *Fourier Transform* of $g(t)$ is $G(f)$, defined by:

$$G(f) = \int_{-\infty}^{\infty} g(t)\exp[-\jmath 2\pi ft]dt\,. \tag{2.24}$$

The *Fourier Transform* is used to convert from the time domain to the frequency domain [30–33], Figure 2.3.

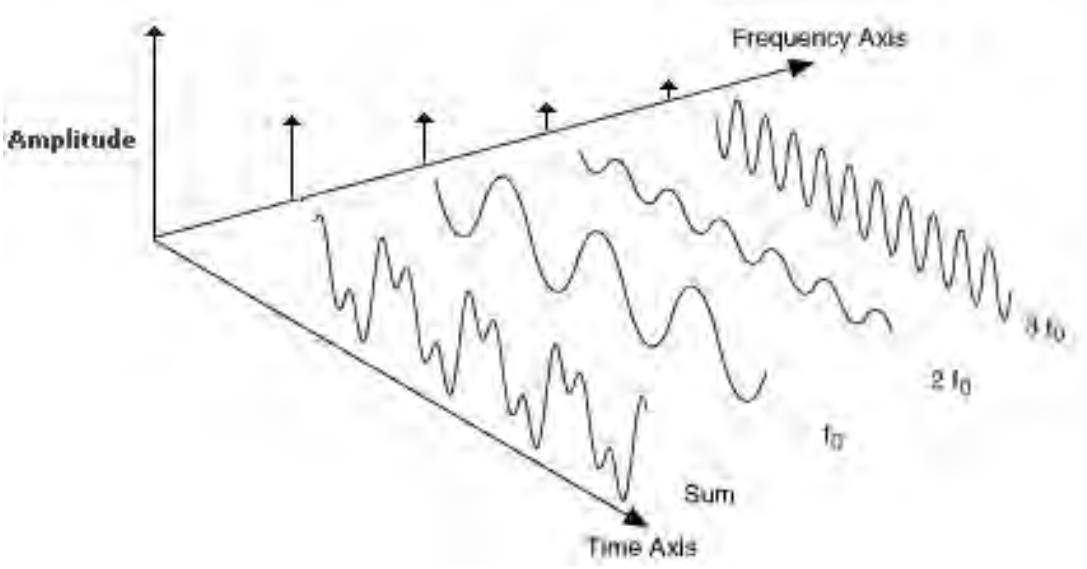

FIGURE 2.3: Time and Frequency domain viewpoints.

The *Fourier Transform* has two important relationships for a Linear system, which are:

$$\Im[f(t-t_0)] = F(w)\exp(-\jmath\omega t_0)\,, \tag{2.25}$$

and

$$\Im[f(t)\exp(\jmath\omega_0 t)] = F(\omega-\omega_0)\,, \tag{2.26}$$

with $\omega = 2\pi f$. Equation (2.25) represents the shift-time property of the *Fourier Transform* while Equation (2.26) is the shift-frequency property of the *Fourier Transform*.

2.7 Impulse Sampling and Harmonics

The main point in Section 2.3 was that the weight of an impulse function represents the sampled number (digital number) at the instant of time that the impulse occurs. The impulse function has some special mathematical relationships [31, 32]:

If $\phi(t)$ is a test function, then:

$$\int_{-\infty}^{\infty}\delta(t)\phi(t)dt = \phi(0)\,, \tag{2.27}$$

which together with the shift property of the impulse function leads to:

$$\int_{-\infty}^{\infty}\delta(t-a)\phi(t)dt = \phi(a)\,. \tag{2.28}$$

Then the Fourier Transform of the impulse function $\Im[\delta(t)]$ is:

$$\Im[\delta(t)] = \int_{-\infty}^{\infty}\delta(t)\exp(-\jmath 2\pi f t)dt = \exp(-\jmath 2\pi f_0) = 1\,. \tag{2.29}$$

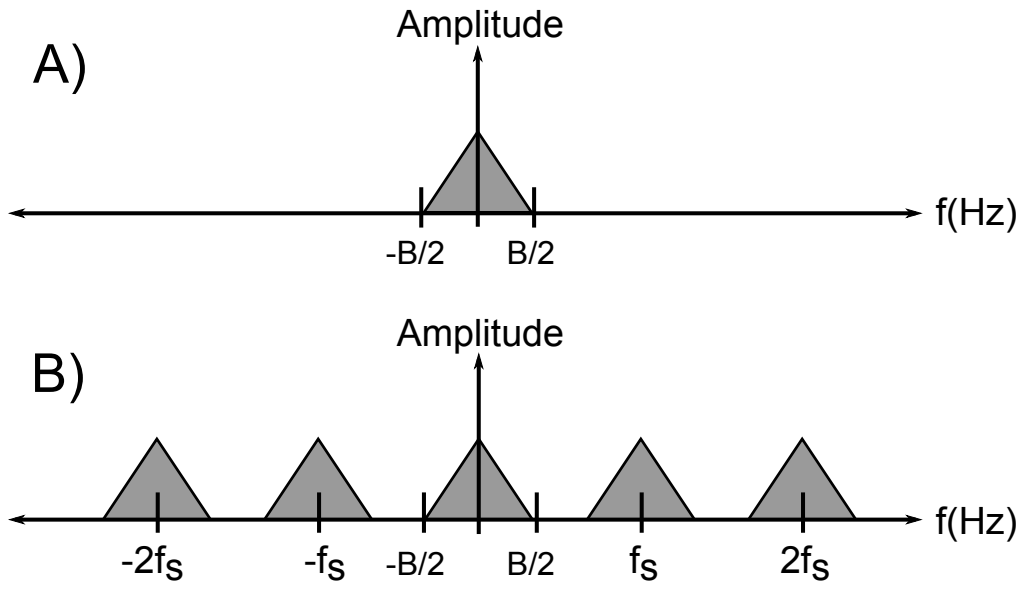

Figure 2.4: The spectrum of the unsampled signal. (B) The spectrum of the sampled signal.

Since the impulse train in Section 2.3 has a period of T, it may be expanded in a Fourier Series. This yields

$$\sum_{n=-\infty}^{\infty} \delta(t - nT) = \frac{1}{T} \sum_{n=-\infty}^{\infty} \exp(\jmath 2\pi n f_0 t)\,. \tag{2.30}$$

This result can be substitute in Equation (2.6) to obtain:

$$x(t)_s = \frac{1}{T} \sum_{n=-\infty}^{\infty} x(t) \exp(\jmath 2\pi n f_0 t)\,. \tag{2.31}$$

Applying the Fourier Transform to both sides of Equation (2.31) the result is:

$$X(\omega) = \frac{1}{T} \sum_{n=-\infty}^{\infty} X(\omega - n\omega_0)\,. \tag{2.32}$$

The spectrum of the impulse sample data signal is shown in Figure 2.4. It is clear that the spectrum of an impulse sampled data signal is a periodic function with frequency F_s. The baseband sampled signal is repeated at integer multiples of the sample frequency commonly called *signal harmonics*. The original signal can be recovered by applying a low-pass filter as it will be shown in the next chapter.

3

Digital Filter on Interferometry

In the Chapter 2 the output $g(t)$ of a linear time-invariant system to any input $f(t)$ can be determined by the convolution with the impulse response $h(t)$ [4, 9, 29]:

$$g(t) = f(t) * h(t)\,, \tag{3.1}$$

in the frequency domain this expression is:

$$G(\omega) = F(\omega)H(\omega)\,. \tag{3.2}$$

The filtering process is equivalent to multiply the input sampled signal $F(\omega)$ by the filter function $H(\omega)$ in the frequency domain. A filter $H(\omega)$ modifies the output frequencies of the input signal $F(\omega)$. The objective of the filtering process is to pass certain frequencies and attenuate others. In the frequency domain, the frequency spectrum of a signal is multiplied by a function which selects what frequency of the signal will pass and what frequencies will be rejected or cancelled [28, 29, 34].

A digital filter separates frequencies. For example, the input signal to a filter could have three different frequencies and the output might contain just two or even one of the frequencies. The best way to describe a filter is a graph, as shown in Figure 3.1. An ideal filter has a square shape, as the dotted line surrounded the gray zone in Figure 3.1. The *passband* all those frequencies included in the output signal without no attenuation. The *stopband* include all those frequencies rejected, amplitude zero and infinite attenuation, at the output signal. The ideal filter has an immediate transition between the *passband* and the *stopband*. This characteristic of the ideal filter is impossible to realize, but a digital filter can come very close.

The output response of the filter depends on the frequency and amplitude of the input signal. The frequency response of real filters differs from an ideal filter in these points:

- There could be undulations in the passband.
- There could be undulations in the stopband.

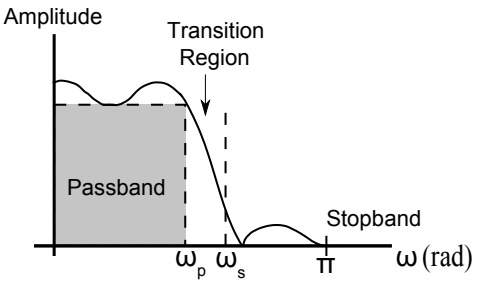

FIGURE 3.1: Ideal and real frequency response graphs of a filter.

- There could be loss in the passband.
- The stopband attenuation is finite.

3.1 Filtering Fringes and Getting Information

The signal recovered by a CCD, in an experimental set-up related to experiments in optical interferometry and more exactly, in *Phase Shifting Interferometry* (PSI), can be mathematically modelled by [35, 36]:

$$g(x,y,t) = a(x,y) + b(x,y)\cos(\phi(x,y) + \omega_0 t)\,, \tag{3.3}$$

where $a(x,y)$ is the background illumination, $b(x,y)$ is the fringe visibility (contrast), $\phi(x,y)$ is the phase at $(t = 0)$ that contains information related to the physical variable to be measured, and $\omega_0 t$ is the temporal sampling period where $t \in \mathbb{Z}$. Equation (3.3) can be rearranged (by using the Euler's formula) and expressed as:

$$g(x,y,t) = a(x,y) + \frac{1}{2}b(x,y)\exp\left(\jmath(\phi(x,y) + \omega_0 t)\right) + \frac{1}{2}b(x,y)\exp\left(-\jmath(\phi(x,y) + \omega_0 t)\right). \tag{3.4}$$

Taking the Fourier Transform of Equation (3.4) the result is [4, 8, 13, 36]:

$$\begin{aligned} G(x,y,\omega) = a(x,y)\delta(\omega) + \frac{1}{2}b(x,y)\exp\left(\jmath\phi(x,y)\right)\delta(\omega-\omega_0) + \\ \frac{1}{2}b(x,y)\exp\left(-\jmath\phi(x,y)\right)\delta(\omega+\omega_0)\,. \end{aligned} \tag{3.5}$$

Figure 3.2 represents the spatial frequency spectra of Equation (3.5). The main objective at this point is to eliminate the background term $a(x,y)$ and one of the terms $\frac{1}{2}b(x,y)\exp\left(\pm\jmath\phi(x,y)\right)\delta(\omega+\omega_0)$ as it is show in Figure 3.1. The signal remained is a complex function in the time domain. The angle of this signal leads to obtain the phase $\phi(x,y)$ contained in Equation (3.4). The filter used to achieve the phase estimation $\hat{\phi}(x,y)$ is a one-side bandpass convolution filter tuned at the temporal frequency carrier $\pm\omega_0$. One-side bandpass filter is commonly called a ***quadrature filter***, shown in Figure 3.1. The ***Quadrature filter*** are complex functions $h(t)$ in time domain or $H(\omega)$ in the frequency domain, its output

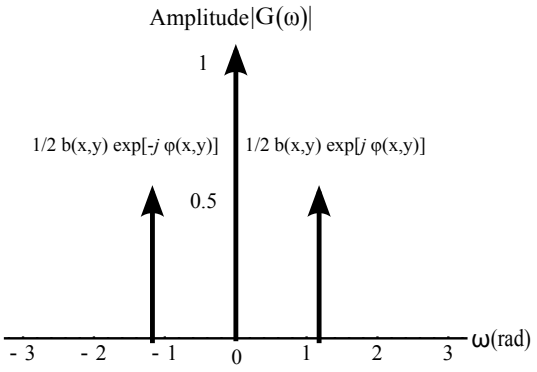

FIGURE 3.2: Spatial frequency spectra of $a(x,y)\delta(\omega) + \frac{1}{2}b(x,y)\exp(\jmath\phi(x,y))\delta(\omega-\omega_0) + \frac{1}{2}b(x,y)\exp(-\jmath\phi(x,y))\delta(\omega+\omega_0)$. The value of ω_0 is $\pi/2$. The frequency variation of the terms $a(x,y)$, $b(x,y)$ and $\phi(x,y)$ are slow compared with the frequency carrier ω_0. Each of the phase terms $\phi(x,y)$ are separated from the background signal by the frequency carrier ω_0.

angle gives the searched phase $\phi(x,y)$. The frequency properties of a quadrature filter in the frequency domain are:

$$H(-\omega_0) = 0 \quad H(0) = 0 \quad H(\omega_0) \neq 0\,, \tag{3.6}$$

or

$$H(-\omega_0) \neq 0 \quad H(0) = 0 \quad H(\omega_0) = 0\,. \tag{3.7}$$

The temporal convolution among interferograms and the *quadrature filter* $h(t) = \Im^{-1}[H(\omega)]$, where $\Im{-}1[\cdot]$, gives as result the complex signal:

$$I(x,y,t) * h(x,y,t) = I(x,y,\omega) * H(\omega) = \frac{1}{2}b(x,y)\exp[\jmath\phi(x,y)]\exp(\omega_0 t)\,. \tag{3.8}$$

Solving for $\phi(x,y)$ and by using Euler's formula($\exp(\jmath\phi(x,y)) = \cos(\phi(x,y)) + \jmath\sin(\phi(x,y))$ the the result is:

$$I(x,y,t) * h(x,y,t) = \frac{1}{2}b(x,y)(\cos(\phi(x,y)+\omega_0 t) + \jmath\sin(\phi(x,y)+\omega_0 t))\,, \tag{3.9}$$

the value of the angle $\hat{\phi}(x,y,t)$ from the complex signal is:

$$\tan(\phi(x,y)+\omega_0 t)) = \frac{\sin(\phi(x,y)+\omega_0 t))}{\cos(\phi(x,y)+\omega_0 t)} = \frac{Im(I(x,y,t)*h(x,y,t))}{Re(I(x,y,t)*h(x,y,t))}\,, \tag{3.10}$$

after some algebraic manipulations, $\hat{\phi}(x,y,t)$ is:

$$\hat{\phi}(x,y,t) = \arctan\left[\frac{Im(I(x,y,t)*h(x,y,t))}{Re(I(x,y,t)*h(x,y,t))}\right] - \omega_0 t\,. \tag{3.11}$$

The latter Equation denotes the capability to estimate the phase $\hat{\phi}(x,y)$ at any time, and usually it is calculated for $t = 0$.

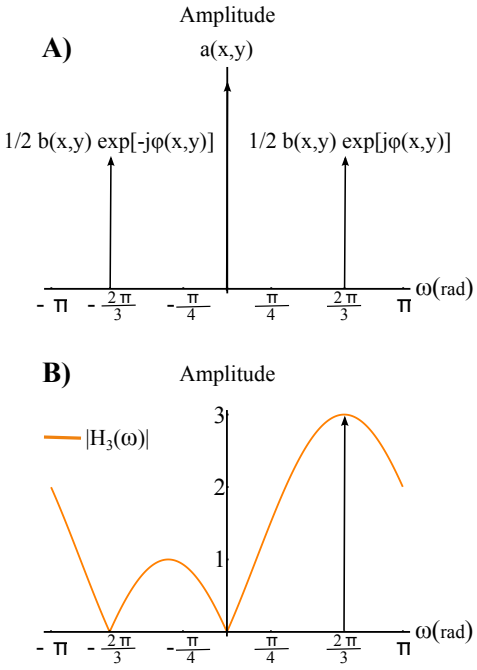

FIGURE 3.3: A)Spatial frequency spectra of $a(x,y)\delta(\omega) + \frac{1}{2}b(x,y)\exp(\jmath\phi(x,y))\delta(\omega - \omega_0) + \frac{1}{2}b(x,y)\exp(-\jmath\phi(x,y))\delta(\omega + \omega_0)$, which is the input signal to the PSA. The value of ω_0 is $2\pi/3$. B) After the filtering process, by using a quadrature filter designed by using the minimum least square, the output single spectrum $\frac{1}{2}b(x,y)\exp(\jmath\phi(x,y))\delta(\omega - \omega_0)$ is selected to pass, while the others two terms of the input signal in A) are blocked. The properties listed in Equation (3.7) are performed as $H(-\omega_0) = 0$, $H(0) = 0$ and $H(\omega_0) \neq 0$. The output signal in the time-domain is $\frac{1}{2}b(x,y)\exp(\jmath\phi(x,y))\exp(\omega_0)t$.

A generalization for the interferogram equations and the *quadrature filter* could be written by using the sampling theory, Section 2.3, as follows [4, 36]:

$$I_n(x,y,nT) = I(x,y,t)\sum_n \delta(t - nT) \text{ with } n = -N,\ldots,0,\ldots,N\,. \tag{3.12}$$

The quadrature filter, as it will be shown in the next chapter, can be written as:

$$h_n(nT) = \exp(\jmath\omega_0 t)\sum_n a_n\delta(t - nT) \text{ with } n = -N,\ldots,0,\ldots,N\,. \tag{3.13}$$

Equations (3.12) and (3.13) are related to the sampling period nT. A *quadrature filter* has the same number of coefficients as the number of interferograms. The coefficients a_n in Equation (3.13) grasp a Fourier Series in the frequency domain, see Equation (2.28). Hence, a *quadrature filter* has a frequency function depicted by the complex terms a_n. The PSA or frequency filter associated, has a Fourier transform $H_n(\omega) = F[h_n(t)]$. The implementation of a temporal convolution between Equation (3.12) and Equation (3.13) results in the following $\hat{\phi}(x,y,0)$:

$$\hat{\phi}(x,y,0) = \arctan\left(\frac{\sum_n b_n \sin(\omega_0 nT)I(x,y,nt)}{\sum_n a_n \cos(\omega_0 nT)I(x,y,nt)}\right)\,. \tag{3.14}$$

The book *Interferogram Analysis for Optical Testing* contains a bunch of PSA based in the number of interferograms and the set value for ω_0.

3.2 Filter Transfer Function of PSA

A basic and easy technique, developed in this thesis work, to construct linear PSA is the successive multiplication of a building blocks which is based in the frequency shifted first-order difference [21]. The mathematical model of this building block is:

$$h(t) = [\delta(t) - \delta(t-1)] \exp(-\jmath\omega_0 t)\,. \tag{3.15}$$

The Fourier transform of Equation (3.15) is:

$$H(\omega) = F[h(t)] = 1 - \exp(\jmath(\omega - \omega_0))\,. \tag{3.16}$$

This filter building block has a zero at frequencies $\omega = -\omega_0$ and $\omega = 0$, and a non zero amplitude signal located at $\omega = +\omega_0$. The minimum PSA is composed by these conditions and hence, the multiplication of the following two first order systems synthesize a *3-step* linear PSA.

$$H_3(\omega) = [1 - \exp(\jmath\omega)][1 - \exp(\jmath(\omega - \omega_0))]\,. \tag{3.17}$$

The construction of $H_3(\omega)$ by the Minimum Least Square [9] technique, implies a value of $\omega_0 = 2{*}\pi/3$. The PSA designed by the Minimum Least Square tuned at $\omega_0 = 2\pi/3$, according to Equation 3.17, has the following response in the frequency domain $H_3(2\pi/3) = 3\exp(-\jmath 0)$. In other case when the frequency carrier is not $\omega_0 = 2\pi/3$ a phase term not equal to zero is present.

Figure 3.1 represents the magnitude of $H_3(\omega)$ designed by Minimum Least Square technique $\omega_0 = 2\pi/N$, in this case $N = 3$, and it has two zeros, one at $\omega = 0$ and the second at $\omega = -2\pi/3$. These two zeros fulfils the minimum requirements for a *3-step* PSA. The size of the output signal is $3(b/2)$ and its piston phase displacement or DC output term is 0. The inverse Fourier transform of $H_3(\omega)$ is:

$$h_3(t) = F^{-1}[H(\omega)] = \delta(t) + (1 + \exp(\jmath\omega_0))\delta(t-1) + \exp(\jmath\omega_0)\delta(t-2)\,. \tag{3.18}$$

The interferometric signal for a *3-step* with temporal carrier ω_0 is expressed according to Equation (3.12) as:

$$I_3(x,y,t) = I(x,y,0)\delta(t) + I(x,y,1)\delta(t-1) + I(x,y,2)\delta(t-2)\,, \tag{3.19}$$

the convolution between $h_3(t)$ and the interferometric signal $I_3(x,y,t)$ gives as result:

$$I_3(x,y,t) * h_3(t) = \begin{array}{lll} I(x,y,0)\delta(t) & +CI(x,y,0)\delta(t-1) & +DI(x,y,0)\delta(t-2) + \cdots \\ I(x,y,1)\delta(t-1) & +CI(x,y,1)\delta(t-2) & +DI(x,y,1)\delta(t-3) + \cdots \\ I(x,y,2)\delta(t-2) & +CI(x,y,2)\delta(t-3) & +DI(x,y,2)\delta(t-4)\,, \end{array} \tag{3.20}$$

ω_0	Filter Complex Response at ω_0
$\pi/3$	$1.73\exp(-\jmath\pi/3)$
$\pi/4$	$1.08\exp(-\jmath\pi/4)$
$\pi/2$	$2.82\exp(-\jmath\pi/2)$
$2\pi/3$	$3\exp(-\jmath 2\pi/3)$
π	0

TABLE 3.1: Filter Complex Response at ω_0 for linear tunable *3-step*. The evaluation of Equation (3.17) at $\omega = -\omega_0$ results in the complex output response of the PSA in the frequency domain.

where $C = -(1+\exp(\jmath\omega_0))$ and $D = \exp(\jmath\omega_0)$. The evaluation at $t = -2$ where the sample elements are maximum results in:

$$|H_3(\omega_0)|\exp(\jmath\Delta_3(\omega_0))\frac{b}{2}\exp(\jmath\hat{\phi}(x,y)) = DI(x,y,0) + CI(x,y,1) + I(x,y,2)\,. \tag{3.21}$$

The *3-step* PSA from Equation (3.21) is:

$$\hat{\phi}(x,y) = \arctan\left(\frac{\sin(\omega_0)(I(x,y,1) - I(x,y,2))}{I(x,y,0) - (1+\cos(\omega_0))I(x,y,1) + \cos(\omega_0)I(x,y,2)}\right)\,. \tag{3.22}$$

The PSA response in the frequency domain is a function of the value ω_0, Table 3.2 shows the *3-step* PSA output response for different values of ω_0.

3.3 Detuned frequency carrier in PSA

The PSA utilizes a minimum of three temporal phase-shifted interferograms to estimate the phase $\hat{\phi}(x,y,0)$. Any PSA is the convolution between the signal $I(x,y,nT)$ and the *quadrature filter* $h(nT)$. The accuracy in the phase estimations depends on the right tuned up between the complex signal $I(x,y,nT)$ and the *quadrature filter* $h(nT)$. When this is not the case, the difference between the temporal carrier used to obtain the interferograms and the assumed value in the PSA will bring an erroneous phase estimation, called *detuning error*. An example of a right tuned up *quadrature filter* with the interferogram is shown in Figure 3.4.

If the frequency carrier ω_0 is not the frequency sampling used to obtain the set of N-interferograms, see Equation (3.12), the *quadrature filter* and the signal of the interferogram are not tuned in the frequency domain. This is illustrated in Figure 3.5. This detuning in the interferogram signal could be due to noise, vibration, or missed calibration in the experimental set up or even in the image acquisition process. When this detuning is present, the output

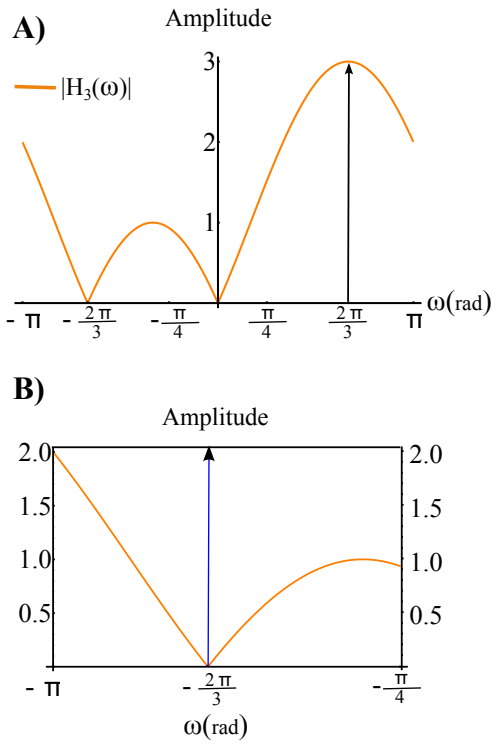

Figure 3.4: A) Single spectrum of the quadrature filter $H_3(\omega, 2*pi/3)$. The filter cancels out the terms of the input signal $a(x,y)\delta(\omega)$ and $\frac{1}{2}b(x,y)\exp[-\jmath\phi(x,y)]\delta(\omega+\omega_0)$ while the term $\frac{1}{2}b(x,y)\exp[\jmath\phi(x,y)]\delta(\omega-\omega_0)$. This is possible because the input signal and the filter are tuned. B) Image zoom around $\omega_0 = -2\pi/3$. It is easy to observe the tuned up relation between the *quadrature filter* and the interferogram signal. The tuned frequency is $|\omega_0|$.

signal as result of the convolution between the *quadrature filter* and the interferogram is:

$$\begin{aligned} G(x,y,\omega)H(\omega) = a(x,y)H(\omega)\delta(\omega) + \frac{1}{2}b(x,y)H(\omega)\exp[\jmath\phi(x,y)]\delta(\omega-\omega_0) \\ + \frac{1}{2}b(x,y)H(\omega)\exp[-\jmath\phi(x,y)]\delta(\omega+\omega_0)\,. \end{aligned} \tag{3.23}$$

And applying the conditions expressed in Equation (3.7), the result in Equation (3.23) must be $\frac{1}{2}b(x,y)H(-\omega)\exp[\jmath\phi(x,y)]$. As it was mentioned before, if an erroneous temporal frequency carrier expressed by: $\omega = \omega_0 + \Delta\omega$ is taken as the sampling frequency, then the result in Equation (3.23) is:

$$\begin{aligned} G(x,y,\omega) = \frac{1}{2}b(x,y)H(-\omega_0-\Delta\omega)\exp[\jmath\phi(x,y)]\delta(\omega-\omega_0-\Delta\omega) \\ + \frac{1}{2}b(x,y)H(\omega_0+\Delta\omega)\exp[-\jmath\phi(x,y)]\delta(\omega+\omega_0+\Delta\omega)\,. \end{aligned} \tag{3.24}$$

The terms of Equation (3.24) can be represented due a phasor diagram, see Figure 3.6. This representation is visually usefull and allows to express the detuning error as $\Delta\phi = \phi' - \phi$,

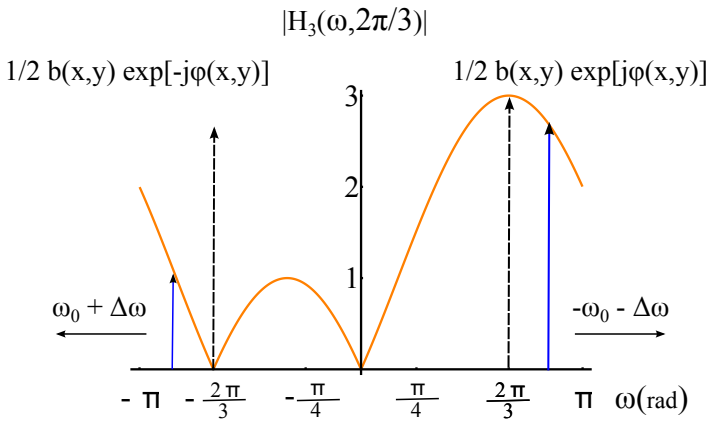

FIGURE 3.5: Single spectrum of the quadrature filter $H_3(\omega, 2*pi/3)$. The filter just cancels out the term of the input signal $a(x,y)\delta(\omega)$ while the terms $\frac{1}{2}b(x,y)\exp[-\jmath\phi(x,y)]\delta(\omega+\omega_0)$ and $\frac{1}{2}b(x,y)\exp[\jmath\phi(x,y)]\delta(\omega-\omega_0)$ are allowed to pass. There is a detuned relation between the *quadrature filter* and the interferogram signal. The conditions in Equation (5.3) are not filled out. The interferograms are not sampled at the frequency $|\omega_0|$ which is the tuned frequency for the filter. The terms $\frac{1}{2}b(x,y)\exp[-\jmath\phi(x,y)]\delta(\omega+\omega_0)$ and $\frac{1}{2}b(x,y)\exp[\jmath\phi(x,y)]\delta(\omega-\omega_0)$ are shifted by a value of $\delta(\omega-\omega_0-\Delta\omega)$ and $\delta(\omega+\omega_0+\Delta\omega)$ respectively.

which is the difference between the desired phase ϕ and the undesired phase $\phi^{'}$. From the phasor diagram and by applying the sinus law to the triangle formed by $H(\omega_0+\Delta\omega)$, $H(-\omega_0-\Delta\omega)$ and $G(\omega)$ it is obtain:

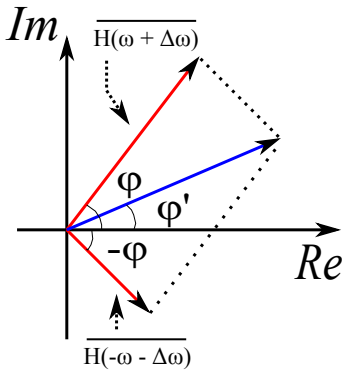

FIGURE 3.6: Phasor representation of Equation (3.24).

$$\frac{H(\omega+\Delta\omega)}{H(-\omega-\Delta\omega)} = \frac{\sin(\phi-\phi^{'})}{\sin(\phi+\phi^{'})}, \tag{3.25}$$

as the deviation $\Delta\omega$ allows to set $\sin(\phi-\phi^{'}) \approx \phi-\phi^{'}$ and $\sin(\phi+\phi^{'}) \approx \sin(2\phi)$, Equation (3.25)

turns in:

$$\phi - \phi^{'} = \frac{H(\omega + \Delta\omega)}{H(-\omega - \Delta\omega)} \sin(2\phi)\,. \tag{3.26}$$

Equation (3.26) can be used to obtain the estimated phase and as it is reported by Mosino *et al* [37], the result for $\hat{\varphi}(x, y, 0)$ is:

$$\hat{\varphi}(x, y, 0) = -\frac{|H(\omega + \Delta\omega)|}{|H(-\omega - \Delta\omega)|} \sin(2\phi(x, y, 0))\,. \tag{3.27}$$

This Equation shows the fact that the detuned phase always has a component which depends on the interferogram fringes frequency having twice the interference fringes which is $\sin(2\phi(x, y, 0))$.

3.4 Break Point for the Thesis Targets

There are a lot of techniques, methods, and analysis of PSA in the literature. Each of them has a particular point of view according to the authors' comprehension in the field of Phase Shifting Interferometry. When user wants to select the best PSA for his application, many times this requires the employment of two or more methods. This situation leads to a complicated and confused assignment. The use of the Linear Theory System for the studying and interpretation of the PSA, originated the establishment of a building block as the framework in design and interpretation of the features wanted in the spectral response. As individual elements, each of this building blocks can be figured out as individual filters working over the signal in a characteristic frequency range. In fact, at the present time it is suitable to construct an *N-step quadrature filter* that can reject one, two, three or more frequencies with the same number of interferograms. This is very useful when the supposition of constant phase-step among the *N-interferograms* is not valid due to a detuning error in the frequency carrier..

4

Design of PSA by Fine-Tuning Spectral Shaping

4.1 Classification of by its PSA Construction

It is worth to mention that PSAs may be clasified in three large groups:

1. Constant phase-step linear PSAs:

   These PSAs are phase estimating formulas in which the phase-step is constant. An example of a linear PSA with constant phase step ($\omega_0 = \pi/2$) is the *5-step* Schwider-Hariharan algorithm [15, 19, 20]:

   $$\widehat{\phi}(x,y) = \arctan \frac{2\left[I\left(-1\right) - I(1)\right]}{2I\left(0\right) - I\left(-2\right) - I\left(2\right)}; \quad \omega_0 = \frac{\pi}{2}\,, \tag{4.1}$$

   where $\widehat{\phi}(x,y)$ is the estimated modulating phase.

2. Variable phase-step linear (*tunable*) PSAs:

   In a tunable phase-step PSA, the explicit appearence of the *phase-step* ω_0 is given. We may generate an infinite number of linear tunable PSAs by selecting a real valued ω_0 within the interval $(0,\pi)$. An example of a *5-step* linear-tunable PSA is [38]:

   $$\widehat{\phi}(x,y)|_{t=0} = \arctan \frac{2\left[I\left(-1\right) - I\left(1\right)\right]\sin\left(\omega_0\right)}{2I\left(0\right) - I\left(-2\right) - I\left(2\right)}\;; \quad \omega_0 \in (0,\pi)\,. \tag{4.2}$$

3. Non-linear *self-tuning* PSAs

   Non-linear self-tuning PSAs is an algorithm that does not need an explicit value of ω_0 in the PSA arctangent ratio. The estimation of the frequency carrier ω_0 is given by an algebraic combination of the interferograms' data. In other words, a formula using the

intensities of the interferograms gives an estimate for ω_0 [8, 16, 39, 40]. Stoilov *et al* designed the followig *5-step* non linear *self-tuning* PSA [18]:

$$\widehat{\phi}(x,y)|_{t=0} = \arctan \frac{2\left[I\left(-1\right) - I\left(1\right)\right]\sqrt{1-\left[\frac{I(-2)-I(2)}{2[I(-1)-I(1)]}\right]^2}}{2I\left(0\right) - I\left(-2\right) - I\left(2\right)} \,. \tag{4.3}$$

Comparing Equation (**??**) with Equation (**??**), we can see that $\sin\left(\omega_0\right)$ is given as the square root of a non-linear algebraic combination of the interferometric data.

It is easy to note that Equation (4.1) is derived from Equation (4.2), by setting ω_0 equal to $\pi/2$; the result is the Schwider-Hariharan linear (constant phase-step) PSA. In turn, Equation (4.3) is an extension of Equation (4.2); the term $\sin\left(\omega_0\right)$ is given by the square root estimator.

The first impression is that linear tunable PSAs are hard to design, but as it will be shown here they are not so difficult to construct them. Once having a mathematical model for a linear tunable PSA (with explicit dependence on ω_0 as in Equation (4.2)), we look for the best carrier ω_0 within the interval$(0,\pi)$ that maximizes the signal to noise ratio of the demodulated phase, see Chapter 5.3.1.

4.2 Spectral analysis of PSI algorithms based on the FTF

For the reader's convenience, we briefly review the FTF approach in PSI [4]. Let us show the standard mathematical model of a set of N phase-shifted interferometric data as

$$I(x,y,t) = \sum_{k=0}^{N-1} \left\{a(x,y) + b(x,y)\cos[\phi(x,y) + \omega_0 k]\right\} \delta(t-k) \,. \tag{4.4}$$

Here the background illumination is $a(x,y)$, the fringe contrast is $b(x,y)$, and the carrier frequency is ω_0 (radians/interferogram). The Fourier transform $F[\cdot]$ of this signal over t is

$$\begin{aligned} I(x,y,\omega) = a\delta(\omega) + \frac{b}{2}\exp[-\jmath\phi]\delta(\omega+\omega_0) \\ + \frac{b}{2}\exp[\jmath\phi]\delta(\omega-\omega_0). \end{aligned} \tag{4.5}$$

To know the phase of interest $\phi(x,y)$ one needs a filter $h(t)$, to wipe out the $a\delta(\omega)$ term and one $b/2$ term. For this purpose, the measured signal $I(t)$ is introduced into a general N-steps PSA as

$$\tan[\phi(x,y)] = \frac{\sum_{k=0}^{N-1} a_k \sin(\omega_0 t) I(k)}{\sum_{k=0}^{N-1} a_k \cos(\omega_0 t) I(k)} \,. \tag{4.6}$$

This PSA may be seen as the following *N-step* of the quadrature filter $h(t)$ tuned at the frequency ω_0 [radians/ per sample],

$$h(t) = \left\{\sum_{k=0}^{N-1} a_k \delta(t-k)\right\} \exp(\jmath\omega_0 t), \qquad H(\omega) = F[h(t)] = \sum_{k=0}^{N-1} a_k \exp(-\jmath k(\omega-\omega_0)) \tag{4.7}$$

The data $I(t)$ in the Equation (4.4) and the quadrature-filter $h(t)$ it may be convolved as,

$$S = [I(t) * h(t)]_{t=N-1} = \sum_{k=0}^{N-1} a_k \exp(\jmath\omega_0 k) I(k) \ . \tag{4.8}$$

The complex number S is the value of $I(t) * h(t)$ evaluated at the middle-point $t = N-1$, where the filter $h(t)$ and the data $I(t)$ are fully overlaped. Finally, the searched phase is $\phi(x, y) = Angle[S]$.

We visualize and determine the exact frequency behaviour of the PSA by its spectrum's amplitude, in other words by plotting $|H(\omega)|$ as [4, 36],

$$|H(\omega)| = |F[h(t)]| = \sqrt{Re(\omega)^2 + Im(\omega)^2} \ . \tag{4.9}$$

Here $H(\omega) = Re(\omega) + \jmath Im(\omega)$, being $Re(\omega)$ and $Im(\omega)$ real-valued functions. The magnitude of $|H(\omega)|$ has the good properties of being invariant to local oscillator's $\exp(\jmath\omega_0 t)$ phase-shifts, and also having a well defined spectral plot for either a symmetric or non-symmetric PSA.

4.3 Characteristic Polynomial (CP) associated to a PSI algorithms

The CP proposed by Surrel [11] is defined from the right hand side of Equation (4.8) as,

$$P(x) = \sum_{k=0}^{N-1} a_k \exp(\jmath\omega_0 k) x^k = \prod_{k=0}^{N-2} (x - d_k) \ . \tag{4.10}$$

$P(x)$ is the x-polynomial function or Characteristic Polynomial (CP). The data $I(k)$ in Equation (4.8) is formally substituted by x^k [11] as it is shown in Equation (4.8). As Surrel shows, it is convenient to express $P(x)$ as a product of $N-1$ monomials $(x - d_k)$, where d_k represents the exact position of the roots of this CP in the unit circle. M roots at d_k means that the PSA is robust enough to detuning at d_k up to order M. Finally, the zeroes at d_k, and their multiplicities are plotted in a CP diagram [11]. The CP diagram is a unit circle where the roots are market. The first order zeroes are plotted as small solid disks, and their multiplicities with greater circles around them [11].

Note that the FTF and the CP analyzing features are related by

$$H(\omega) = \exp(-\jmath(N-1)\omega) P(\exp(\jmath\omega)) \ . \tag{4.11}$$

Given that the x-polynomial $P(x)$ is closely related with the Z-transform, the later mathematical equivalence obtained in Equation (4.11) has been known for decades in the theory of the digital linear systems [3].

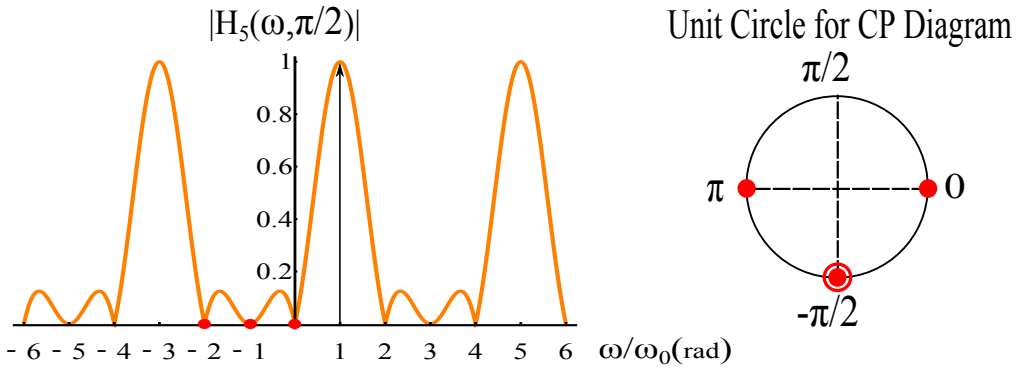

FIGURE 4.1: Magnitude of $H_5(\omega)$ given by Equation (4.14), and its CP diagram in the unit circle. The PSA spectral plot $H_5(\omega)$ has two first-order zeroes at 0 and π, and a second-order one at $-\pi/2$.The PSA spectral plot shows, with circles, where are located the zeros of the quadrature filter in order to create a link with the plot of the CP diagram.

4.4 Fine-tuning spectral-zeroes for approximating a desired PSA spectrum

A first-order linear system that generates a spectral zero at ω_0 is [3]

$$h(t) = [\delta(t) - \delta(t-1)] \exp(-\jmath\omega_0 t) \; . \tag{4.12}$$

This may be seen by Fourier transforming $h(t)$ as

$$H(\omega) = F[h(t)] = 1 - \exp(\jmath(\omega - \omega_0)) \; . \tag{4.13}$$

This is the basic building block of our zero-based, spectral-shaping PSAs design. Note that, the equivalent x-monomial is $P(x) = x - \exp(-\jmath\omega_0)$. We will combine several first-order building blocks (Equation (4.13)), and freely tuning their zeroes, to approximate a desired PSA spectral template.

As a first example, suppose that a *5-step* PSA's is wanted, which has a flatter rejecting-band around $-\pi/2$. This is the spectral description of the 5-step Schwider-Hariharan (SH) PSA, see Figure 4.3 [11, 15]. The SH-PSA has the following FTF

$$\begin{aligned} H_{SH}(\omega) = (1 - \exp(\jmath\omega)[(1 - \exp(-\jmath(\omega + \pi/2)]^2 \\ (1 - \exp(-\jmath(\omega + \pi))) \; . \end{aligned} \tag{4.14}$$

The x-polynomial of the SH-PSA is $(x-1)(x-\jmath)^{1/2}(x+1)$. The CP diagram and the plot of $H_{SH}(\omega)$ are shown in Figure 4.1. This PSA has a second-order zero at $-\pi/2$, and two first-order zeroes at 0 and π. The second-order zero gives a robustness detuning at $-\pi/2$.

The *5*-step SH described in Equation (4.14), is just one example of all the possibles PSA that can be designed. Now, it is possible to evoke the potential, described in Equation (4.13), in freely moving the zero location in a PSA filter. By moving one of zero placed at $-\pi/2$,

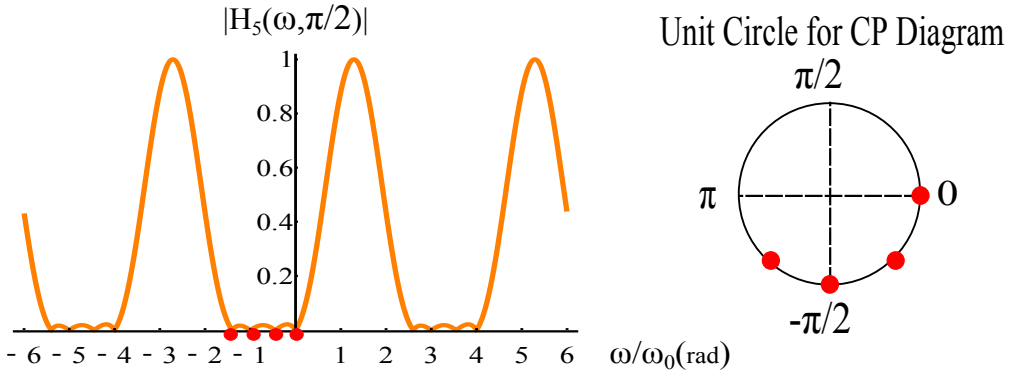

Figure 4.2: Magnitude of $H_5(\omega)$ and its CP diagram. The PSA spectrum has been considerably flattened around $\pi/2$ with respect to $H_{SH}(\omega)$ for the same measured interferograms. From the CP diagram alone, the spectral shape outside the 4 zeroes shown is absent. On the other hand, the plot of $H_5(\omega)$ shows it clearly. One must be aware of the small ripples within the stop band. The PSA spectral plot shows, with circles, where are located the zeros of the quadrature filter in order to create a link with the plot of the CP diagram.

and the one at π, it can be possible to flatten the response around $-\pi/2$. This is done while gauging the $H_5(\omega)$ plot. A feasible non-symmetric PSA with a frequency carrier $\omega_0 = \pi/2$ is:

$$\begin{aligned} H_5(\omega) = [1 - \exp(\jmath\omega)][1 - \exp(-\jmath(\omega + 0.45\omega_0))] \\ [1 - \exp(-\jmath(\omega + \omega_0))][1 - \exp^{-\jmath(\omega+1.4\omega_0)}] \, . \end{aligned} \tag{4.15}$$

The equivalent (CP) x-polynomial is $P_5(x) = (x-1)(x-\exp(-\jmath 0.225\pi))(x-\exp(-\jmath 0.5\pi))(x-\exp(-\jmath 0.7\pi))$. The CP diagram and the plot of $H_{SH}(\omega)$ are shown in Figure 4.2. By inverse Fourier transforming $H_5(\omega)$, or expanding $P_5(x)$, (both options being equally easy by using any computer numerical program) we find the desired *non-symmetric* PSA as:

$$\tan(\phi) = \frac{-2.4I(\pi/2) + 2.9I(\pi) + 0.57I(3\pi/2) - I(2\pi)}{I(0) - 1.2I(\pi/2) - 2.3I(\pi) + 2.7I(3\pi/2) - 0.23I(2\pi)}. \tag{4.16}$$

In Figure 4.3 we show an application for our modified PSA (Equation (4.16)) to simulated speckle-like interferograms. The 5 interferograms along with the wrapped phase obtained from (Equation (4.16)) are shown in Figure 4.3.

Let us continue with another example, a *9-step* PSA. We want high detuning robustness, (6 zeroes) at $\omega_0 = \pi/2$, and also robustness to bias illumination's variation; 2 zeroes at $\omega = 0$. Figure 4.4 shows the CP diagram of $P_9(x) = (x-1)^2(x+\jmath)^6$, and the plot of $|P_9 = \exp(\jmath\omega)|$.

Let us spread the zeros of $P_9(\exp(\jmath\omega))$ around $-\omega_0$. A flatter than $P_9(\exp(\jmath\omega))$ spectral response is obtained by spreading-out its 8 available zeroes. This is done while gauging the

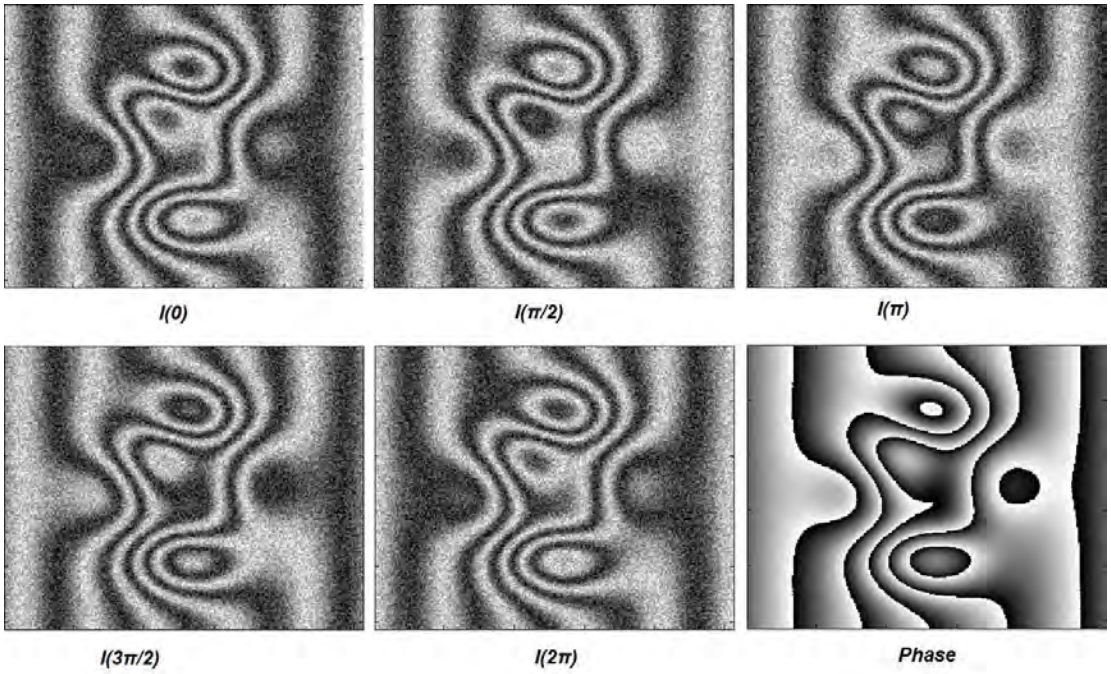

FIGURE 4.3: Simulated speckle-like interferograms applied to the modified PSA (Equation (4.16)). The 5 interferograms used in Equation (4.16) may also be used for the *SH*-PSA. However the PSA detuning robustness is higher in the modified PSA (Equation (4.16)) than in the *SH*-PSA (Equation (4.14)).

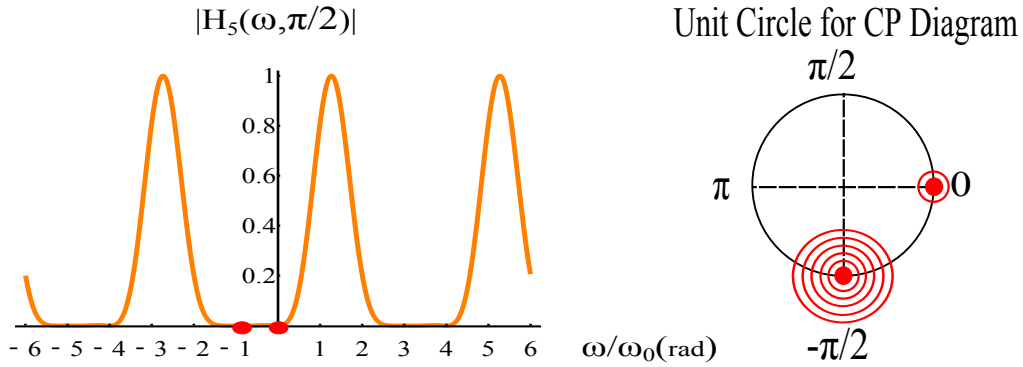

FIGURE 4.4: Magnitude of $P_9 \exp(\jmath\omega)$ and its CP diagram. The resulting spectral rejection band is wide, being of 6^{th} order around ω_0 and of 2^{nd} order around the origin. The PSA spectral plot shows, with circles, where are located the zeros of the quadrature filter in order to create a link with the plot of the CP diagram.

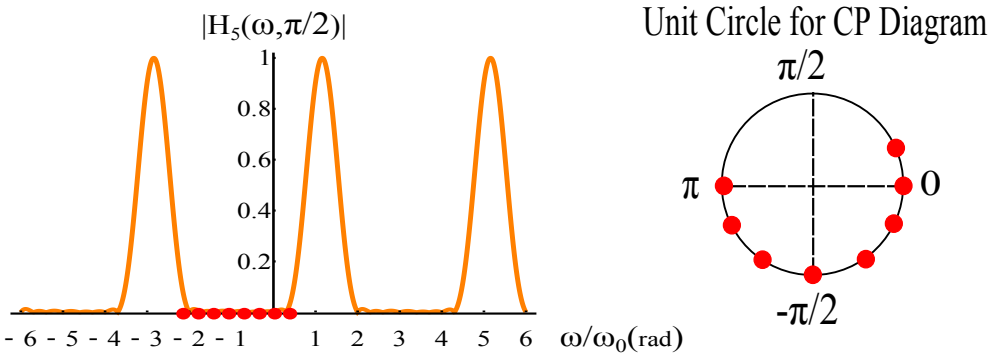

Figure 4.5: CP diagram, and magnitude of $H_9(\omega)$. The resulting PSA's spectral shape has been further flattened with respect to $P_9(\exp(\jmath\omega))$ around ω_0 and around the origin. From the CP diagram alone, one may only wonder about the spectral amplitude outside the displayed zeroes, making almost impossible the fine-tuning task performed herein. The PSA spectral plot shows, with circles, where are located the zeros of the quadrature filter in order to create a link with the plot of the CP diagram.

$|H_9(\omega)|$ plot. Another suitable expression for nine *non-symmetric* PSA:

$$\begin{aligned} H_9(\omega) = &[1-\exp(-\jmath(\omega-0.3\omega_0))][1-\exp(-\jmath(\omega))][1-\exp(-\jmath(\omega+0.3\omega_0))] \\ &[1-\exp(-\jmath(\omega+0.6\omega_0))][1-\exp(-\jmath(\omega+\omega_0))][1-\exp(-\jmath(\omega+1.4\omega_0))] \\ &[1-\exp(-\jmath(\omega+1.7\omega_0))][1-\exp(-\jmath(\omega+2\omega_0))]. \end{aligned} \tag{4.17}$$

As Figure 4.5 shows, the final results of a fine tuned is the flattened of the rejected band with respect to that of $P_9(\exp(\jmath\omega))$. The 8 zeroes have been spread out around the unit circle. The designer may wide even more the rejection band at a cost of tolerating bigger ripples; the signal amplitude at ω_0 is 82 times bigger than a signal placed at $\omega = 0.2\omega_0$. This plot clearly shows the detailed spectral amplitude including the small ripples which cannot be seen in the CP diagram. The Invese Fourier transform of $H_9(\omega)$ allows to find $h_9(t)$ and from it, the searched *9-step non-symmetric* PSA.

4.5 Signal-to-Noise power ratio (S/N) in PSA designs

Given that the CP diagram is blind to the continuous spectral amplitude, we cannot see if our PSA would perform better against noise with a slight change of the data carrier ω_0, as it will be shown in the next chapter. By looking at Figure 4.5 (for example) we see that the desired signal at $\omega_0 = \pi/2$, does not coincide with the spectra's peak. Let us calculate the S/N power-ratio at ω_0, and at its peak $1.16\omega_0$ [4],

$$S/N(\omega_0) = \frac{|H_9(\omega_0)|^2}{\frac{1}{2\pi}\int_{-\pi}^{\pi}|H_9(\omega)|^2 d\omega} = 5.3\,, \quad S/N(1.16\omega_0) = \frac{|H_9 1.16\omega_0)|^2}{\frac{1}{2\pi}\int_{-\pi}^{\pi}|H_9(\omega)|^2 d\omega} = 6.6. \tag{4.18}$$

That means that increasing our carrier ω_0 from 0.5π (radians/sample) to 0.58π one obtains a 24.5% gain in the S/N power-ratio, *i.e.* $(6.6/5.3) = 1.245$. This suggested carrier of $1.16\omega_0$ will change the aspect of the continuous plot of $H_9(\omega)$) in Figure 4.5. In contrast, observing the CP diagram alone, it is impossible to see where the location of the PSA's spectral maximum is. In addition, the F&K spectral plot [23] cannot be used because it does not exist for *non-symmetrical* PSA.

5

N-step linear phase-shifting algorithms with optimum signal to noise phase demodulation

5.1 Phase shifting interferometry corrupted by additive Noise

The standard mathematical model for an interferogram corrupted by additive noise is:

$$I(x,y,t) = a(x,y,t) + b(x,y,t)\cos[\phi(x,y) + \omega_0 t] + n(x,y,t)\,,\ \ t \in (0,1\ldots)\,. \tag{5.1}$$

In this Equation, $a(x,y)$ is the background illumination, $b(x,y)$ is the contrast of the fringes, $\phi(x,y)$ is the phase being measured, ω_0 is the phase step (or frequency carrier) used, and finally $n(x,y,t)$ is an additive corrupting noise. The latter is considered Gaussian, stationary, white, with a flat power spectral density $S(\omega) = \eta/2$. We know that additive noise is not the only kind of interferometric measuring noise. There is also the multiplicative or phase noise that is attributable to speckles because of the coherent laser illumination used. However, once a linear low pass filter is applied for cleaning up the fringe data, the multiplicative noise turns into additive Gaussian noise by the law of large numbers [19]. Moreover, after using several times a 3x3-averaging filter, one normally ends up with reasonably clear (still corrupted by some additive noise) fringes [19] as modelled in Equation (5.1). The signal in Equation (5.1) can be decomposed into complex components as follows:

$$I(t) = a + \frac{b}{2}\exp[\jmath(\phi + \omega_0 t)] + \frac{b}{2}\exp[-\jmath(\phi + \omega_0 t)] + n(t)\,. \tag{5.2}$$

The explicit dependence (x,y) of the signal has been omitted for clarity. To obtain the searched analytical signal $(b/2)\exp[\jmath(\phi + \omega_0 t)]$ it needs to filter out the low-frequency

background $a(x,y)$, and the complex signals $(b/2)\exp[-\jmath(\phi+\omega_0 t)]$. Assuming that the complex term at $+\omega_0$ is kept, the linear PSA (a quadrature filter) must have a frequency transfer function (FTF) $H(\omega)$ with at least the following frequency response [4, 36]

$$H(-\omega_0)=0 \quad H(0)=0 \quad H(\omega_0)\neq 0\,. \tag{5.3}$$

Applying this FTF function $H(\omega)$ to the interferograms the following complex output signal is obtained [4, 36]:

$$F^{-1}[I(\omega)H(\omega)]_{t-0}=I(t)*h(t)|_{t=0}=\frac{b}{2}H(\omega_0)\exp(\omega_0)\exp(\jmath\phi)+\bar{n}\exp(\jmath\Phi)\,. \tag{5.4}$$

$F[\cdot]$ is the Fourier transform operator and $F^{-1}[\cdot]$ its inverse. The symbol $*$ denotes the one-dimensional (over t) convolution, and $h(t)$ is the quadrature's filter impulse response associated with the PSA, having FTF $H(\omega)=F[h(t)]$ [36]. The term $\bar{n}\exp(\jmath\Phi)$ is a complex random variable associated to the Gaussian additive output noise. Finally, Φ is a random (phase noise) process uniformly distributed within the interval $[0,2\pi]$ [15]. The estimated phase at $t=0$ is given by the linear PSA associated to $h(t)$ as [4]:

$$\widehat{\phi}(x,y)=\left.\frac{Im[I(x,y,t)*h(t)]}{Re[I(x,y,t)*h(t)]}\right|_{t=0}, \tag{5.5}$$

where the operators $Re[\cdot]$ and $Im[\cdot]$ take the real and the imaginary part of their argument. The hat over $\hat{\phi}(x,y)$ denotes its estimated value that may differ from the true phase $\phi(x,y)$ stated in Equation (5.1).

In the next section, we describe two spectral linear tunable PSA models. The first analyzed algorithm is the tunable 3-step linear PSA, which is the simplest and probably the most frequently used algorithm. Later on, we analyze PSAs with 5, 7, 27 step using another tunable spectral model finding the best carrier ω_0 that maximizes the S/N ratio. Other linear tunable N-step PSA spectral models can be easily defined, although they may have different optimal carriers ω_0.

5.2 Linear tunable phase shifting algorithms

As was mentioned in the introduction of this chapter, to find the best ω_0 that maximizes the S/N ratio we need linear tunable PSA. In this work it is shown how to construct linear tunable PSAs by combining first-order digital filter, or by combining second-order digital linear filters. Repeated convolutions of these first or second order digital filters lead to higher order linear PSAs.

5.2.1 Linear tunable PSAs by combining first-order digital filter

We first construct linear tunable PSAs by combining two simple first-order digital linear filters. The basic mathematical model for these first-order filters are:

$$h_1(t)=\delta(t)-\delta(t-1)\,, \tag{5.6}$$

$$h_1(t,\omega_0) = [\delta(t) - \delta(t+1)]\exp(-\jmath\omega_0 t)\,, \tag{5.7}$$

where $\delta(t)$ is the Dirac delta function, and $\jmath = \sqrt{-1}$. The FTF of these basic models are:

$$F[h_1(t)] = H_1(\omega) = 1 - \exp(\jmath\omega)\,, \tag{5.8}$$

$$F[h_1(t,\omega_0)] = H_1(\omega,\omega_0) = 1 - \exp[-\jmath(\omega-\omega_0)]\,, \tag{5.9}$$

the combination of several first order blocks leads to the desired N-step linear tunable PSA's FTF [22]. A spectral model for high-order N-step linear tunable PSA may be given by:

$$H_N(\omega,\omega_0) = H_1^n(\omega)H_1^m(\omega,\omega_0)\ ;\ N = n+m+1\,, \tag{5.10}$$

where the number of possible steps N is $3,\ 4,\ 5, 6, ..., n+m+1$. The simplest example of this construction model is a 3-step linear tunable PSA. This filter has the following FTF:

$$H_3(\omega,\omega_0) = H_1^1(\omega)H_1^1(\omega,\omega_0) = (1-\exp(\jmath\omega))[1-\exp(\jmath(\omega_0-\omega))]\,, \tag{5.11}$$

and taking the inverse Fourier transform $F^{-1}[\cdot]$ of Equation (5.10), $h_3(t,\omega_0) = F^{-1}[H_3(\omega,\omega_0)]$ one obtains the complex impulse response of the linear 3-step PSA tuned at ω_0 as follows:

$$h_3(t,\omega_0) = -\delta(t-1) + \delta(t) + \exp(i\omega_0)\delta(t) - \exp(i\omega_0)\delta(t+1),\ \omega_0 \in (0,\pi)\,. \tag{5.12}$$

By using the Equation (4.6) and the Equation (5.12) one obtains a 3-step linear PSA tuned at ω_0 as [41]:

$$\widehat{\phi}(x,y)|_{t=0} = \arctan\left\{\frac{\sin(\omega_0)[I(0)-I(1)]}{-I(-1)+I(0)+\cos(\omega_0)[I(0)-I(1)]}\right\}\ ;\quad \omega_0 \in (0,\pi)\,. \tag{5.13}$$

The equation above represents a *3-step* linear *tunable* PSA and the spectral amplitude $|H_3(\omega,\omega_0)|$ is shown in Figure 5.1 for $\omega_0 = 2\pi/3$. The complex harmonics rejected by this linear tunable PSA are clearly identified from the plot. In this particular frequency span the complex harmonics rejected are: $(..., -6, -4, -3, -1,\ 2,\ 3,\ 5,\ 6, ...)$.

5.2.2 Linear tunable PSAs by combining second-order digital filters

In this subsection we construct linear tunable PSAs by combining two second-order digital linear filters. Repeated convolutions of these two (second-order) filters leads to higher-order linear PSAs. In other words, several convolutions of these two simple building blocks generate arbitrarily high order linear tunable PSAs [42]. The mathematical forms of these second-order filters are:

$$h_2(t) = \jmath\,[\delta(t-1) - \delta(t+1)]\,, \tag{5.14}$$

$$h_2(t,\omega_0) = -\exp(-\jmath\omega_0)\delta(t-1) + 2\delta(t) - \exp(\jmath\omega_0)\delta(t+1)\,. \tag{5.15}$$

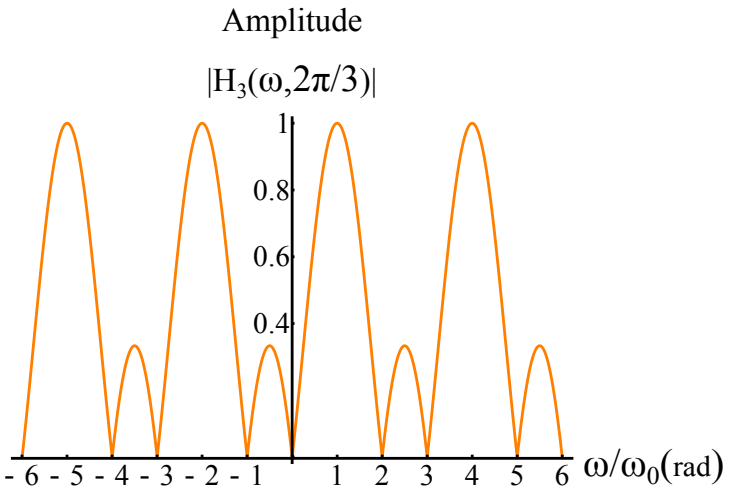

FIGURE 5.1: The *3-step* linear PSA, tuned at $\omega = 2\pi/3$. It is shown in this chapter that the optimum carrier that minimizes the demodulated phase-noise of this linear PSAs is $2\pi/3$. In this particular figure the complex harmonic rejected are: $(..., -6, -4, -3, -1,\ 2,\ 3,\ 5,\ 6, ...)$.

The frequency transfer function (FTF) of these filters are:

$$H_2(\omega) = F[h_2(t)] = -2\ \sin(\omega)\,, \tag{5.16}$$

$$H_2(\omega, \omega_0) = F[h_2(t, \omega_0)] = 2 - 2\cos(\omega - \omega_0)\,. \tag{5.17}$$

$H_2(\omega)$ filters out the background $a(x, y)$ at $\omega = 0$, and also the signals components at $\omega = (..., -2\pi, -\pi, 0,\ \pi,\ 2\pi, ...)$, this is shown in Figure 5.1. On the other hand, the filter $H_2(\omega, \omega_0)$ can be frequency tuned to any ω_0 (within $(0, \pi)$), removing the complex signal at $\omega = -\omega_0$ and letting to pass its conjugate at $\omega = \omega_0$. The simplest spectral product of these two building blocks gives the FTF of a 5-step tunable PSA:

$$H_5(\omega, \omega_0) = H_2(\omega)H_2(\omega - \omega_0)\ ; \quad \omega_0 \in (0, \pi)\,, \tag{5.18}$$

This spectrum complies with Equation (3.6), which gives the minimum conditions for a valid linear tunable PSA. Taking the inverse Fourier transform of Equation (3.6), one obtains the complex impulse response of a 5-step linear tunable quadrature filter $h_5(t, \omega_0) = F^{-1}[H_5(\omega, \omega_0)]$

$$\begin{aligned} h_5(t, \omega_0) = &-\jmath \exp(-\jmath\omega_0)\delta(t-2) + 2\jmath\delta(t-1) + \\ &\jmath \exp(-\jmath\omega_0)\delta(t) - \exp(\jmath\omega_0)\delta(t) - \\ &2\jmath\delta(t+1) + \jmath \exp(\jmath\omega_0)\delta(t+2))\,. \end{aligned} \tag{5.19}$$

As this equation shows, the impulse response $h_5(t, \omega_0)$ depends on the choice of the phase-step ω_0 used. Finally, according to Equation (4.6), one obtains a linear 5-step PSA tuned at

ω_0 as

$$\widehat{\phi}(x,y)|_{t=0} = \arctan\left\{\frac{2[I(-1)-I(+1)]+\cos(\omega_0)[I(+2)-I(-2)]}{\sin(\omega_0)[2I(0)-I(+2)-I(-2)]}\right\}. \tag{5.20}$$

Note that this linear tunable *5-step* PSA reduces to the Schwider-Hariharan linear PSA for $\omega_0 = \pi/2$ [15, 18]. A useful spectral-model for higher order linear PSA is obtained by combining $H_2(\omega)$ and higher powers of $H_2(\omega,\omega_0)$, increasing the detuning robustness of the PSA at ω_0. In other words, a higher power in $H_2(\omega,\omega_0)$ flattens the linear PSA spectral response at ω_0 [4, 21]. Therefore, the spectral model for the high-order *N-step* linear tunable PSAs considered in this work has the form:

$$H_N(\omega,\omega_0) = H_2(\omega)[H_2(\omega-\omega_0)]^{\frac{N-5}{2}+1},\ N=5,\ 7,\ 9,\ 11,\ldots, \tag{5.21}$$

For example, one can obtain the spectrum of a $N = 27$-step PSA tuned at $\omega_0 = \pi/2$ as

$$H_{27}(\omega,\pi/2) = H_2(\omega)[H_2(\omega-\pi/2)]^{12}. \tag{5.22}$$

The Figure 5.2 shows the spectra of a 5-step, 7-step, and 27-step linear PSAs all tuned at $\omega_0 = \pi/2$, obtained by Equation (5.21). The left side complex signal at $\omega = -\pi/2$ is zero for all 5, 7 and 27-step linear PSAs, while being transparent at $\omega = \pi/2$. The 27-step linear PSA spectrum is (almost) flat-zero for $\omega \in (-\pi, 0)$ as a consequence it has very small detuning error [4, 21]. In these particular cases, the rejected complex harmonics are: $(..., -8, -6, -5, -4, -2, -1,\ 2,\ 3,\ 4,\ 6,\ 7,\ 8, ...)$. Also, as Figure 5.2 shows, these quadrature filters are very robust to detuning at these harmonics. Finally, the linear tunable PSA that results from this N-step spectral model as given by Equation (5.21) applied to our set of N phase-shifted interferograms $I_N(x,y,t)$ is:

$$\hat{\phi}(x,y) = \arctan\left\{\frac{Im[h_N(t,\omega_0) * I_N(x,y,t)]}{Re[h_N(t,\omega_0) * I_N(x,y,t)]}\bigg|_{t=0}\right\};\quad \omega_0 \in (0,\pi), \tag{5.23}$$

where $h_N(t,\omega_0) = F^{-1}[H_N(\omega,\omega_0)]$.

5.3 Optimum phase-step to obtain the maximum S/N ratio gain

This section describes the objective of this Chapter, in order to obtain the optimal carrier ω_0^{opt} for a linear tunable PSAs to obtain the best signal to noise (S/N) power ratio. As far as we know, the optimal value ω_0^{opt} for a given linear PSA spectral model that renders the least noisy demodulated phase has not been published previously to our knowledge.

We assume that the output power noise $\bar{n}$ in Equation (5.4) is substantially less than the amplitude of the output complex signal, i.e., $\bar{n} << H(-\omega_0,\omega_0)b/2$ which is the additive low-noise approximation. This condition is normally fulfilled when the interferograms are low-pass filtered to remove some noise [13, 24]. Under these circumstances, the S/N power ratio of the output phase can be demonstrated to be [24]

$$\left[\frac{S}{N}(\omega_0)\right]_{output} = \frac{|H(\omega_0)|^2}{\frac{1}{2\pi}\int_{-\pi}^{\pi} H(\omega,\omega_0)H^*(\omega,\omega_0)d\omega}\left[\frac{S}{N}\right]_{input} = G(\omega_0)\left[\frac{S}{N}\right]_{input}, \tag{5.24}$$

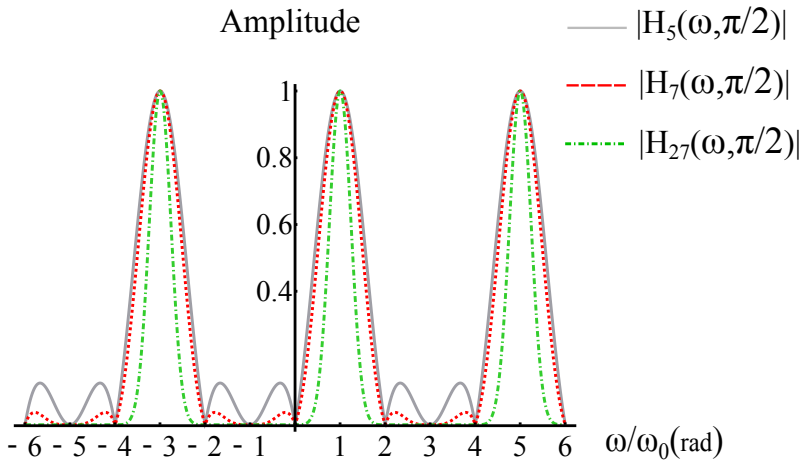

FIGURE 5.2: Linear tunable PSAs with 5, 7 and 27-steps with spectral model given by Equation (5.21). These quadrature filters remove the DC term at $\omega = 0$ and the complex frequency component at $\omega = -\pi/2$. The rejected complex harmonics are: $(..., -8, -6, -5, -4, -2, -1, \ 2, \ 3, \ 4, \ 6, \ 7, \ 8, ...)$. These harmonics rejections are robust to detuning.

where $(S/N)_{input}$ is the interferogram's signal to noise power ratio. $H(\omega, \omega_0)$ stands for the filter's spectrum (which depends on the interferogram's carrier ω_0), and $H^*(\omega, \omega_0)$ stands for its complex conjugate. $G(\omega_0)$ is the algorithm's (S/N) power gain. Note that the S/N algorithm's gain $G(\omega_0)$ is a function of the carrier frequency ω_0 alone. In other words, given a mathematical spectral model for linear tunable PSA providing $H(\omega, \omega_0)$ we may choose the carrier ω_0 which maximizes this power ratio gain $G(\omega_0)$ in Equation (5.24).

5.3.1 Optimum ω_0 to obtain the best (S/N) ratio for a 3-step linear PSA

Owing to its wide use, let us first analyze the spectrum of a 3-step linear tunable PSA and find the optimum carrier that minimizes its demodulated phase noise. The 3-step linear PSA tuned at ω_0, has the following formula [41, 43]:

$$\widehat{\phi}(x,y) = \arctan\left\{\frac{[1-\cos(\omega_0)][I(x,y,-1)-I(x,y,1)]}{\sin(\omega_0)[2I(x,y,0)-I(x,y,-1)-I(x,y,1)]}\right\}; \quad \omega_0 \in (0,\pi)\,. \tag{5.25}$$

The temporal impulse response associated with this linear tunable PSA is [4, 5]

$$h_3(t,\omega_0) = \sin(\omega_0)[2\delta(0)-\delta(t+1)-\delta(t-1)] + \jmath\{[1-\cos(\omega_0)][\delta(t-1)-\delta(t+1)]\}\,, \tag{5.26}$$

and its FTF $H(\omega, \omega_0)$ is (in this case real):

$$H_3(\omega,\omega_0) = F[h_3(t,\omega_0)] = 2\sin(\omega_0)[1-\cos(\omega)] - 2[1-\cos(\omega_0)]\sin(\omega);\ \omega_0 \in (0,\pi)\,. \tag{5.27}$$

N-step	Filter Spectral Response (FTF)
3	$H_3(\omega,\omega_0) = \sin(\omega_0) - \sin(\omega_0-\omega) - \sin(\omega)$
5	$H_5(\omega,\omega_0) = \sin(\omega_0) - \sin(\omega_0-2\omega) - 2\sin(\omega)$
7	$H_7(\omega,\omega_0) = \sin(\omega_0) + \sin(2\omega_0-3\omega) - \sin(\omega-2\omega) - \sin(2\omega_0-\omega) - \sin(\omega)$
27	$H_{27}(\omega,\omega_0) = \sin(\frac{\omega_0-\omega}{2})^{24}\sin(\omega)$

Table 5.1: Filter Transfer Function for the 3, 5, 7, and 27-step linear tunable PSA models used in this chapter.

N-step	Linear tunable PSA
3	$\hat{\phi}_3(\omega,\omega_0) = \arctan\left(\frac{I(-1)-I(1)+\cos(\omega_0)(I(1)-I(-1))}{\sin(\omega_0)(I(-1)+2I(0)-I(1)}\right)\ ;\ \omega_0 \in (0,\pi)$
5	$\hat{\phi}_5(\omega,\omega_0) = \arctan\left(\frac{-\cos(\omega_0)(I(-2)+I(2)+I(-1)-I(1)}{\sin(\omega_0)(I(-2)+I(0)-I(2)}\right)\ ;\ \omega_0 \in (0,\pi)$
7	$\hat{\phi}_7(\omega,\omega_0) =$ $\arctan\left(\frac{\cos(2\omega_0)(I(-3)+I(3)-I(-1)+I(1)+\cos(\omega_0)(I(2)-I(-2))+3(I(-1)-I(1)}{\sin(2\omega_0)(I(-3)+I(3)-I(1)-I(-1))+\sin(\omega_0)(2I(0)-I(2)-I(-2))}\right)\ ;$ $\omega_0 \in (0,\pi)$

Table 5.2: PSA in time domain for the 3, 5, 7, and 27-step models used in this chapter.

Finally, using Equation (5.24) one obtains the S/N ratio gain $G(\omega_0)$ for a 3-step algorithm as follows:

$$G(\omega_0)_{\widehat{\phi}} = \frac{|H_3(\omega_0)|^2}{\frac{1}{2\pi}\int_{-\pi}^{\pi}|H_3(\omega,\omega_0)|^2\,d\omega};\quad \omega_0 \in (0,\pi)\,. \tag{5.28}$$

This last equation states the importance of having a linear tunable PSA in order to find the best tuning frequency ω_0 within the interval$(0,\pi)$. Equation (5.28) shows that the *S/N* ratio gain $G(\cdot)$ depends only on ω_0; therefore setting the derivative of this equation (with respect to ω_0) equal to zero to obtain the optimum ω_0^{opt} which renders the *S/N* power ration gain $G(\omega_0)$ at maximum. In the case of the *3-step* linear PSA, the optimum phase-shift is:

$$\frac{d\,G(\omega_0)}{d\omega_0}|_{\omega_0^{opt}=2\pi/3} = 0\,. \tag{5.29}$$

This corresponds to the optimal carrier frequency $\omega_0^{opt} = 2\pi/3$.

Figure 5.1 shows the FTF, $H_3(\omega, 2\pi/3)$, corresponding to the optimum-carrier 3-step linear PSA. This linear PSA filters out the complex signal at $\omega = -2\pi/3$, while the complex signal at $\omega = 2\pi/3$ is allowed to pass. With this result it is now absolutely certain that a carrier of $2\pi/3$ is the best choice to obtain the cleanest demodulated phase for a 3-step linear PSA corrupted by additive noise. Table 5.3.1 shows the FTF for the 3, 5, 7, and 27-step linear tunable PSA models used in this chapter. Table 5.3.1 shows the PSAs for the 3, 5, and 7-step FTFs in Table 5.3.1).

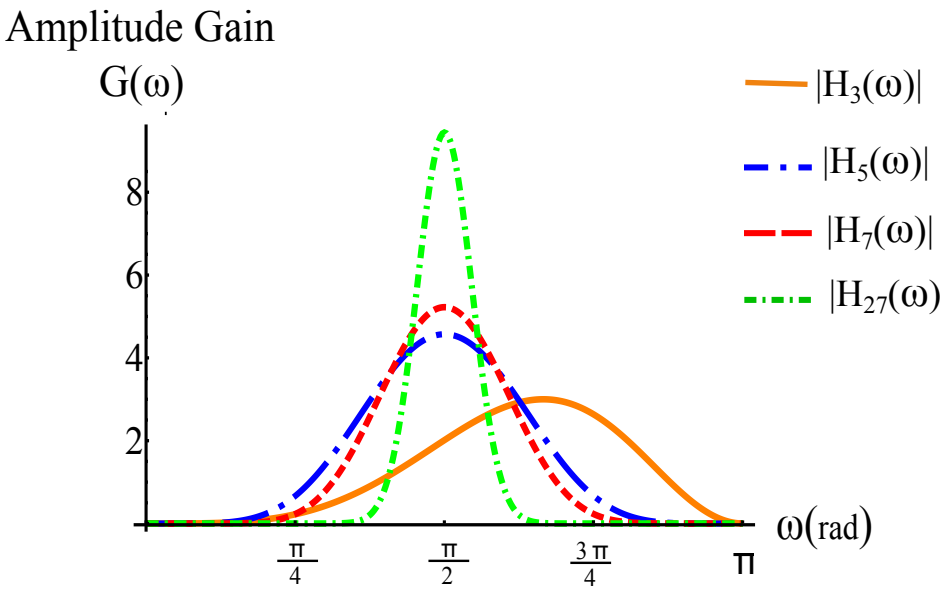

FIGURE 5.3: This figure shows the best frequency carrier through the S/N analysis proposed in this paper.

5.3.2 Optimum phase-step to obtain the maximum S/N gain in high-order linear tunable PSAs

The main purpose of this sub-section is to calculate the optimum temporal carrier ω_0^{opt} from Equation (5.24). Using these second-order filters we obtain the spectra for the 5, 7, and 27-step spectra in Table 5.3.1. The optimum carrier ω_0^{opt} is the one that gives the lowest noise in the phase demodulation process for the linear *N-step* PSA spectral model in Equation (5.21). Figure 5.3 shows four plots corresponding to the $G(\omega_0)$ ratio gain of 3, 5, 7, and 27 step linear tunable PSAs. The $G(\omega_0)$ power-ratio gain depends solely on the carrier frequency ω_0 (see Equation (5.24)). Higher order linear PSAs, modeled by Equation (5.21), $H_N(\omega,\omega_0) = H_2(\omega)H_2(\omega,\omega_0)^{(N-5)/2+1}$, all have their maximum signal to noise gain $G(\cdot)$ at $\omega_0^{opt} = \pi/2$

$$G(\pi/2)_{maximum} = \frac{|H_N(\pi/2)|^2}{\frac{1}{2\pi}\int_{-\pi}^{\pi}|H_N(\omega,\pi/2)|^2\,d\omega}; \quad \omega_0 = \frac{\pi}{2}\,. \tag{5.30}$$

The step-angle of $\pi/2$ is a frequently chosen value in experimental work. Figure 5.3 also shows the intuitive result that, the more steps we have, the higher (optimum) S/N ratio is obtained. From Equation (5.20), we see that for N = 5-steps, and $\omega_0 = \pi/2$ we obtain the Schwider-Hariharan PSA. Therefore, the Hariharan-Schwider linear PSA uses the best possible carrier within its spectral model in Equation (5.21).

6
Conclusions

We have presented a zero-based, fine-tuning, spectrum-shaping technique for designing *N-steps* PSA, based on the visualization and gauging of its continuous FTF spectral magnitude $|H(\omega)|$. This technique gives more possibilities to approximate a target spectrum while keeping the size N of the PSA unchanged. This PSA design method starts by specifying a desired PSA spectrums template. Afterwards, the available $(N-1)$ first-order zeroes are freely moved (fine-tuned), to approximate it. Finally, the inverse transform of the FTF$[h(t)]$ is found, and from it the desired (in general non-symmetric) PSA. It is important to remark that given the option of freely move the PSAs $(N-1)$ zeroes, the result is non-symmetric PSAs. These non-symmetric PSAs cannot be analyzed using the F&K spectral-plotting technique.

Finally do not forget that the target PSA spectrum may be determined by taking the Fourier transform of actual interferometric measurements of the kind of fringes being analyzed. This real-data spectral estimation and the desired phase noise-rejection are the key to estimate how many samples (N) a given PSA will need and also where its $(N-1)$ zeroes may be located.

This Thesis introduces a simple technique to find the optimum phase-shift ω_0 which maximizes the signal to noise ratio *(S/N)* on the demodulated phase for linear tunable PSA. This holds true whenever the corrupting interferogram noise is additive, white, and Gaussian. To apply our procedure, one needs a linear tunable PSA spectral model to vary ω_0 and keep the one that maximizes the $G(\omega_0)$ ratio in Equation 5.24. The particular spectral models used in this paper are those in Equation (5.10) and Equation 5.21. These two spectral models were substituted into Equation (5.24), and the best carrier ω_0 that maximizes the S/N ratio gain, $G(\omega_0)$ is chosen. This optimization was applied to 3, 5, 7, and 27-step linear tunable PSAs. We have found that for the case of a 3-step linear PSA, the carrier that maximizes the $G(\omega_0)$ ratio is $\omega_0^{opt} = 2\pi/3$, while for the spectral model in Equation 5.21, the best $G(\omega_0)$ ratio gain is obtained for $\omega_0^{opt} = \pi/2$. This optimizing procedure can be easily extended to other linear tunable PSA spectral models not considered here. Note the important fact that, the optimum value for depends on the PSA spectral model chosen. For example, one may have two *5-step* linear tunable PSAs with different spectral model, having possibly two

different optimum carriers that optimize the signal to noise ratio.

A

Appendix A

A.1 Waves by Sine and Cosine Waves

a = Table[0.5*Sin[(2*Pi*2*t)/10], t, 0, 10, 0.01];
b = Table[0.1*Sin[(2*Pi*4*t)/10], t, 0, 10, 0.01];
c = Table[0.1*Sin[(2*Pi*6*t)/10], t, 0, 10, 0.01];

index = Table[t, t, 0, 10, 0.01];

ListLinePlot[a + b + c, DataRange − > 0, 10, ImageSize − > 800, PlotStyle − > Thick]

A.2 Basic Linear Block Construction Definition

bloque[wo_]:=$\frac{1}{\sqrt{2\pi}} - \frac{\mathrm{Cos}[w-\mathrm{wo}]}{\sqrt{2\pi}} + \frac{i\mathrm{Sin}[w-\mathrm{wo}]}{\sqrt{2\pi}}$;

A.3 Tunable Filter Construction

f1s = TrigReduce[bloque[0] ∗ bloque[−a] ∗ bloque[−1.4 ∗ a]bloque[−0.6 ∗ a]];

absf1s = TrigReduce[(ComplexExpand[Re[f1s]])^2 + (ComplexExpand[Im[f1s]])^2];

ListLinePlot[Table[absfSH, {w, −Pi, Pi, 0.1}], DataRange → {−Pi, Pi},
PlotStyle → {{Thickness[0.005], Orange}}, ImageSize → 1100,
AxesLabel->{Style[ω/ω_0Times, FontSize → 50],
Style[$H_5(\omega, \pi/2)$Times, FontSize → 50]}Ticks → {{−10, −5, −1, 1, 5, 10}, Automatic},
TicksStyle → Directive[Times, FontSize → 45], GridLines → {{Pi/2/(Pi/2)}, None},
GridLinesStyle → Directive[Thick, Gray],
AxesOrigin → {0, 0}, AxesStyle → Thickness[0.005]]

A.4 Numerical Evaluation of SNR

potenciaf1s = (1/(2Pi)) ∗ Integrate[absf1s, {w, −Pi, Pi}];

magnitudf1s = absf1s/.w → a;

snrf1s = Table[magnitudf1s/potenciaf1s, {a, 0, Pi, 0.01}];

potenciafSH = (1/(2Pi)) ∗ Integrate[absfSH, {w, −Pi, Pi}];

magnitudfSH = absfSH/.w → a;

snrfSH = Table[magnitudfSH/potenciafSH, {a, 0, Pi, 0.01}];

ListLinePlot[{snr, snrfSH}, DataRange → {0, Pi},
PlotStyle → {{Thickness[0.005], Orange}, {Thickness[0.005],
Blue}}, ImageSize → 1100, AxesLabel->{Style[ω, Times,
FontSize → 50], Style[SNR, Times, FontSize → 50]},
TicksStyle → Directive[Times, FontSize → 45],
AxesOrigin → {0, 0}, AxesStyle → Thickness[0.005]]

References

[1] J. Schmit and K. Creath. *Extended averaging technique for derivation of error-compensating algorithms in phase-shifting interferometry,.* Appl. Opt. **34(19)**, 3610 (1995). vii

[2] J. H. Bruning, D. R. Herriott, J. E. Gallagher, D. P. Rosenfeld, A. D. White, and D. J. Brangaccio. *Digital wavefront measuring interferometer for testing optical surfaces and lenses.* Appl. Opt. **13(11)**, 2693 (1974). vii

[3] J. G. Proakis and D. G. Manolakis. *Digital Signal Processing* (Pretice Hall, 2006). vii, 2, 3, 5, 27, 28

[4] M. Servin, J. C. Estrada, and J. A. Quiroga. *The general theory of phase shifting algorithms.* Opt. Express **17(24)**, 21867 (2009). vii, 1, 2, 15, 16, 18, 26, 27, 31, 34, 37

[5] D. J. Bone. *Fourier fringe analysis: the two-dimensional phase unwrapping problem.* Appl. Opt. **30**, 3627 (1991).

[6] J. R. Fienup. *Phase retrieval algorithms: a comparison.* Appl. Opt **21**, 2758 (1982). vii

[7] K. G. Larkin and B. F. Oreb. *Design and assessment of symmetrical phase-shifting algorithms.* J. Opt. Soc. Am. A **9(10)**, 17401748 (1992). 2

[8] M. Servin, J. L. Marroquin, and F. J. Cuevas. *Demodulation of a single interferogram by use of a two-dimensional regularized phase-tracking technique.* Appl. Opt. **36(19)**, 4540 (1997). 16, 26

[9] D. Malacara, M. Servin, and Z. Malacara. *Interferogram Analysis for Optical Testing* (Taylor & Francis, 2005). 1, 2, 15, 19

[10] J. A. Quiroga, A. Gonzalez-Cano, and E. Bernabeu. *Phase unwrapping algorithm based on an adaptive criterion.* Appl. Opt. **34**, 2560 (1995).

[11] Y. Surrel. *Design of algorithms for phase measurements by the use of phase stepping.* Appl. Opt. **35(1)**, 51 (1996). 1, 2, 3, 27, 28

[12] M. Takeda, H. Ina, and S. Kobayashi. *Fourier transform method of fringe-pattern analysis for computer-based topography and interferometry.* JOSA A. **72**, 156 (1982). vii

[13] M. Servin, J. Estrada, and J. Quiroga. *Spectral analysis of phase shifting algorithms.* Opt. Express. **17(19)**, 16423 (2009). vii, 1, 16, 37

[14] C. A. Gonzalez, A. Davila, and J. G. Garnica. *Noise reduction of temporal phase unwrapping for 3d shape reconstruction using a quality map.* In J. C. Gutierrez-Vega, J. Davila-Rodriguez, and C. Lopez-Mariscal, eds., *Sixth Symposium Optics in Industry*, vol. 6422 of *Proc. SPIE* (2007). vii

[15] P. Hariharan, B. F. Oreb, and T. Eiju. *Digital phase-shifting interferometry: a simple error-compensating phase calculation algorithm.* Appl. Opt **26(13)**, 2504 (1987). 1, 2, 25, 28, 34, 37

[16] K. G. Larkin. *Efficient nonlinear algorithm for envelope detection in white light interferometry.* J. Opt. Soc. Am. A **13(4)**, 832 (1996). 26

[17] D. W. Phillion. *General methods for generating phase-shifting interferometry algorithms.* Appl. Opt. **36(32)**, 8098 (1997). 1

[18] G. Stoilov and T. Dragostinov. *Phase-stepping interferometry: five-frame algorithm with an arbitrary step.* Opt. Lasers Eng **28**, 414 (1997). 26, 37

[19] J. Schwider, R. Burow, K. E. Elssner, J. Grzanna, R. Spolaczyk, and K. Merkel. *Digital wave-front measuring interferometry: some systematic error sources.* App **22(21)**, 3421 (1983). 2, 25, 33

[20] J. Schwider, O. Falkenstorfer, H. Schreiber, H. Zoller, and N. Streibl. *New compensating four-phase algorithm for phase-shift interferometry.* Opt. Eng. **32(8)**, 1883 (1993). vii, 2, 25

[21] A. Gonzalez, M. Servina, J. Estrada, and H. Rosu. *N-step linear phase-shifting algorithms with optimum signal to noise phase demodulation.* Journal of Modern Optics **58(14)**, 1278 (2011). viii, 19, 37

[22] A. Gonzalez, M. Servin, J. C. Estrada, and J. A. Quiroga. *Design of phase-shifting algorithms by fine-tuning spectral shaping.* Opt. Ex **19(11)**, 10692 (2011). viii, 35

[23] K. Freischlad and C. L. Koliopoulos. *Fourier description of digital phase-measuring interferometry.* J. Opt. Soc. Am. A **7(4)**, 542551 (1990). 1, 2, 32

[24] Y. Surrel. *Additive noise effect in digital phase detection.* Appl. Opt. **36(1)**, 271 (1997). 1, 37

[25] P. Groot. *Derivation of algorithms for phase-shifting interferometry using the concept of a data-sampling window.* Appl. Opt. **34(22)**, 4723 (1995). 2

[26] J. Schmit and K. Creath. *Window function influence on phase error in phase-shifting algorithms.* Appl. Opt. **35(28)**, 5642 (1996). 2

[27] J. Burke. *Extended averaging phase-shifting schemes for fizeau interferometry on high-numerical aperture spherical surfaces.* In *Proc. of SPIE* (2010). 2

[28] H. Hsu. *Analisis de Fourier* (Pre, 1998). 5, 6, 15

[29] B. P. Kumar. *Digital signal processing laboratory* (CRC Press Book, 2005). 6, 15

[30] K. Iizuka. *Engineering optics* (Springer series in optical sciences, 1985). 6, 11

[31] J. W. Goodman. *Introduction to Fourier Optics* (The McGraw - Hill Companies, Inc., Stanford University, 1988). 7, 8, 9, 12

[32] A. VanderLugt. *Optical signal processing* (Wiley, 2005). 9, 12

[33] E. Hecht. *Optics* (Addison-Wesley, 2001). 11

[34] K. Ogata. *Discrete-Time control system* (Pretice Hall, 1995). 15

[35] K. J. Gasvik. *Optical Metrology* (John wiley & Sons, 2002). 16

[36] D. Malacara and B. J. thompson. *Handbook of optical engineering* (Marcel Dekker, Inc., 2001). 16, 18, 27, 34

[37] J. Mosio, M. Servin, J. Estrada, and J. Quiroga. *Phasorial analysis of detuning error in temporal phase shifting algorithms.* Opt. Express **17(7)**, 5618 (2009). 23

[38] P. Carré. *Installation et utilisation du comparateur photoelectrique es interferetiel du bureau international des poids et measures.* Bureau International des Poids et Measures **2**, 13 (1966). 25

[39] J. Novak. *Five-step phase-shifting algorithms with unknown values of phase shift.* Optik **2**, 63 (2003). 26

[40] Q. Kemao, S. Fangjun, and W. Xiaoping. *Determination of the best phase step of the carr algorithm in phase shifting interferometry.* Measurement Science and Technology **11**, 1220 (2000). 26

[41] D. Malacara. *Optical Shop Testing* (Wiley, 2007). 35, 38

[42] J. C. Estrada, M. Servin, and J. A. Quiroga. *Easy and straightforward construction of wideband phase-shifting algorithms for interferometry.* Opt. Lett. **34(4)**, 413 (2009). 35

[43] J. C. Estrada, M. Servin, and J. A. Quiroga. *A self-tuning phase-shifting algorithm for interferometry,.* Opt. Express. **18(3)**, 2632 (2010). 38